THE JOURNAL OF PHYSICAL CHEMISTRY A

Article

pubs.acs.org/JPCA

Solvent Dependent Switching of ^{3}MLLCT and ^{1}IL Luminescent States in [ClRe(CO)$_3$(Bathocuproinedisulfonate)]$^{2-}$: Spectroscopic and Computational Study

Hector H. Martinez Saavedra,[†] Fabricio Ragone,[†] Gustavo T. Ruiz,[†] Pedro M. David Gara,*[,‡] and Ezequiel Wolcan*[,†]

[†]Instituto de Investigaciones Fisicoquímicas Teóricas y Aplicadas (INIFTA, UNLP, CCT La Plata-CONICET), Diag. 113 y 64, Sucursal 4, C.C. 16, (B1906ZAA) La Plata, Argentina

[‡]Centro de Investigaciones Ópticas (CONICET-CIC) and UNLP, Cno. Centenario e/505 y 508, C.C. 3 (1897), La Plata, Argentina

ABSTRACT: Steady state and time-resolved luminescence experiments and calorimetric studies, as well as time-dependent density functional theory calculations performed on [ClRe(CO)$_3$(Bathocuproinedisulfonate)]$^{2-}$, show that the photophysical properties of the Re(I) anionic complex are determined by the balance between intraligand (^{1}IL) and metal–ligand-to-ligand charge transfer (^{3}MLLCT) excited states. In organic solvents, ^{3}MLLCT states prevail and the usual expected behavior is observed: bathochromic shift of the emission maximum, a reduced luminescence quantum yield and the shortening of the excited-state lifetime upon increasing the polarity of the solvent. In addition, singlet oxygen ($^1O_2$) is generated with high quantum yields ($\Phi_\Delta \approx 0.5$ in CH_3CN) due to the quenching of the ^{3}MLLCT luminescence by $^3O_2$. The total quenching rate constant of triplet state by oxygen, k_q, reach values between 2.2 and 2.4 × 10^9 M^{-1} s^{-1} for the organic solvents studied. In CH_3CN, the fraction of triplet states quenched by O_2 which yield $^1O_2$, $f^T_{O_2}$, is nearly unity. In aqueous solution, where no singlet oxygen is generated, the luminescence of the Re(I) complex is of ^{1}IL character with a emission quantum yield (Φ_{em}) strongly pH dependent: $\Phi_{em,(pH=2)}/\Phi_{em,(pH=10)} \approx 5.6$. The variation of the pH of the solution tunes the photophysical properties of the Re(I) complex by changing the relative amount of the different species existing in aqueous solutions: [ClRe(CO)$_3$(BCS)]$^{2-}$, [(OH)Re(CO)$_3$(BCS)]$^{2-}$ and [(H$_2$O)Re(CO)$_3$(BCS)]$^-$. TD-DFT calculations show that the percentage of charge transfer character of the electronic transitions is substantially higher in the organic solvents than in aqueous solutions, in agreement with the increase of ^{1}IL character of HOMO in [(H$_2$O)Re(CO)$_3$(BCS)]$^-$ relative to [ClRe(CO)$_3$(BCS)]$^{2-}$.

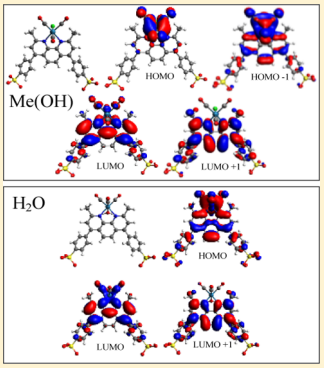

INTRODUCTION

Luminescent organometallic rhenium(I)-tricarbonyl complexes coordinating polypyridine ligands have attracted researchers endeavors for nearly four decades, as they show exceptionally rich excited-state behavior and redox chemistry as well as thermal and photochemical stability.[1,2] Consequently, they have been applied in broad research areas such as electron transfer studies,[3] solar energy conversion,[4−6] and catalysis,[7] as luminescent sensors,[8−10] molecular materials for nonlinear optics[11,12] and optical switching,[7] and as biological labeling reagents and noncovalent probes for biomolecules and ions.[13−15] Depending on the nature of the axial X ligand *fac*-ReX(CO)$_3$(α-diimine) complexes are often strong luminophores, either in fluid solutions or in low-temperature glasses. The accessible excited states, Re(I) to α-diimine metal-to-ligand charge transfer (MLCT), metal–ligand-to-ligand charge transfer (MLLCT), ligand-to-ligand charge transfer (LLCT), and/or intraligand (IL) excited states, are generally involved with the observed luminescence of these complexes at room temperature. In most of the cases, the observed luminescence is of ^{3}MLCT (or rather ^{3}MLLCT) character. However, ^{3}IL or ^{1}IL emission has also been identified in some systems.[14,16] A careful manipulation of the energetic separation of the two emissive states, by changing both the polypyridine ligands and temperature, can control the relative dominance of ^{3}MLCT and IL emission. One of the major disadvantages of *fac*-ReX(CO)$_3$(α-diimine) complexes when applied to biological media is connected to their usually very low solubility in water at physiological pH. In fact, there are a very limited number of water-soluble *fac*-ReX(CO)$_3$(α-diimine) complexes[17−24] compared to the huge number of Re(I) carbonyl–diimine complexes reported to be soluble exclusively in organic solvents. In previous work, we have characterized a pair of water-soluble Re(I) tricarbonyl complexes, one of them including a biological relevant ligand like pterin in its structure.[24,25] In this paper, we study the photophysical properties of a *fac*-ReX(CO)$_3$(α-diimine) complex bearing the water-soluble ligand Bathocuproinedisulfonic acid disodium salt (BCS), namely [ClRe(CO)$_3$(BCS)]$^{2-}$. Because BCS is charged and not membrane permeable, it is commonly used in

Received: July 10, 2014
Revised: September 17, 2014
Published: September 18, 2014

cell studies.[26] The attractive intrinsic photophysical properties common to many Re(I) complexes, such as large Stokes shifts, long luminescence lifetimes and resistance to photobleaching, make these excellent candidates for applications in cell imaging. We study the photophysical properties of the Re(I) complex in organic solvents as well as in aqueous media, using laser-induced optoacoustic spectroscopy (LIOAS), steady-state and time-resolved luminescence techniques and time-dependent density functional theory (TD-DFT) calculations. In the organic solvents, ^{3}MLLCT states govern the photophysical properties of the Re(I) complex with the usual expected behavior: emission shows a bathochromic shift, reduced luminescence quantum yield, and shortened excited-state lifetime upon increasing the polarity of the solvent. Besides, the quenching of the ^{3}MLLCT luminescence by molecular oxygen leads to singlet oxygen generation with high quantum yields ($\Phi_\Delta \approx 0.5$ in CH_3CN). The total quenching rate constant of triplet state by oxygen, k_q, reach values between 2.2 and 2.4 $\times$ 10^9 M^{-1} s^{-1} for the organic solvents studied. In aqueous solution, where no singlet oxygen is generated, the luminescence of the Re(I) complex is of ^{1}IL character with a emission quantum yield (Φ_{em}) strongly pH dependent. Thus, the balance between ^{1}IL and ^{3}MLLCT excited states, which tune the photophysical properties of the Re(I) complex, is governed by the pH dependent replacement of Cl^- by H_2O in its structure. This generates a reduction of the percentage of charge transfer in the relevant singlet−singlet electronic transitions which lead to the population of the emitting ^{1}IL and ^{3}MLLCT excited states, as revealed by TD-DFT calculations. Consequently the equilibrium between ^{3}MLLCT and ^{1}IL is inclined toward the latter in aqueous solutions and the luminescence of the Re(I) complex is governed by ^{1}IL states. Indeed, the photophysical properties of the Re(I) complex are those of the coordinated BCS, with a pH-dependent fluorescence quantum yield similar to the one of the free ligand—though modulated by the positive charge of the metal center—and not detectable generation of singlet oxygen.

EXPERIMENTAL PART

Materials. The anionic complex $[ClRe(CO)_3(BCS)]^{2-}$ was available from previous work.[27] Spectrograde and HPLC grade acetonitrile (J. T. Baker), methanol (MeOH, Sigma-Aldrich) and ethanol (EtOH, Sigma-Aldrich) were used without further purification. 2-Hydroxybenzophenone, phenalenone, New Coccine, D_2O, NaOH, and $HClO_4$ were purchased from Sigma-Aldrich at the highest purity available and were used as received. Deionized water (>18 MΩ cm^{-1}, < 20 ppb of organic carbon) was obtained with a Millipore system.

Photophysical Measurements. UV−vis spectra were recorded on a Shimadzu UV-1800 spectrophotometer. Emission spectra were obtained with a computer-interfaced Near-IR Fluorolog-3 Research Spectrofluorometer, and were corrected for differences in spectral response and light scattering. Solutions were deaereated with O_2-free nitrogen in a gastight apparatus before recording the spectra.

Emission quantum yields, Φ_{em}, were calculated with eq 1, by using solutions of a reference compound with a known quantum yield of emission, Φ_{ref}

$$\Phi_{em} = \left(\frac{A_{ref}}{A_s}\right)\left(\frac{I_s}{I_{ref}}\right)\left(\frac{n_s}{n_{ref}}\right)^2 \Phi_{ref} \quad (1)$$

In eq 1, n_s and n_{ref} are the refractive indexes of the optically diluted solutions (A_s and $A_{ref} < 0.1$) containing the sample and the reference compound, respectively. A solution of Rhodamine B in ethanol was used as a reference with $\Phi_{ref} = 0.69$. The areas under the emission spectra of the sample and Rhodamine B were used as a relative measure of the respective intensities of the luminescence, I_s and I_{ref}, where I is the integral of the emission spectrum and A is the absorbance of the sample or reference at the excitation wavelength. Lifetime measurements were performed using the time-correlated single-photon counting (TCSPC) unit of the Fluorolog-3 with 341 nm NanoLEDs excitation source.

Photoacoustic measurements were performed by using a setup already described.[28] Basically, a Q-Switched Nd:YAG laser (Surelite II, Continuum, 7 ns fwhm) operating at 355 nm was used as excitation source. The fluence of the laser pulses was varied using a neutral density filter, and the energy values were measured with a pyroelectric energy meter (Laser Precision Corp. RJ7620 and RJP-735). The laser beam was shaped by a 1 mm diameter pinhole in front of the cuvette, so that the resolution time in our experimental setup, τ_R, was ca. 800 ns.[29] The detecting system consisted of a 4 mm thick × 4 mm in diameter homemade ceramic piezoelectric transducer (PZT), pressed against a cuvette side wall parallel to the laser beam direction. The detected acoustic signals were amplified, digitized by a digital oscilloscope (TDS 3032, Tektronix), and stored in a personal computer for further treatment of the data. The cuvette was in a temperature-controlled (±0.1 °C) holder. New Coccine or 2-Hydroxybenzophenone were used as calorimetric reference (CR) compounds in the buffer and in CH_3CN solutions, respectively.[30,31] A at λ_{exc} for the CR and the sample were matched within 5%. The signals generated by 64 laser shots for the sample and the CR each time under the same conditions, were averaged to obtain a better signal-to-noise ratio. The absorption spectrum of the solution was checked before and after each set of laser shots, in order to detect possible sample degradation. Solutions were deaerated by bubbling N_2 or O_2 for 15 min before each experimental run. Given an excited species with a lifetime of τ, if $\tau \leq {}^1/_5\tau_R$ then this species releases its heat content as prompt heat. On the other hand, when $\tau > 5\tau_R$ the excited species function as heat storage within the time resolution of the LIOAS experiment.

The peak to peak amplitude of the first optoacoustic signal (H) is related to the fraction of the excitation laser fluence (F) absorbed by the sample by eq 2,[29] which was used for the handling of the LIOAS signals

$$H = K\alpha F(1 - 10^{-A}) \quad (2)$$

where the experimental constant K contains the thermo-elastic parameters of the solution as well as instrumental factors. A and α represent, respectively, the absorbance of the sample at the excitation wavelength and the fraction of the energy released to the medium as prompt heat.

The efficiency of the Re(I) complex toward singlet oxygen sensitization was assessed by the direct measurement of the $^1O_2$ ($^1\Delta_g$) near-infrared luminescence. After the irradiation of aerated solutions of the complex the generation of $^1O_2$ ($^1\Delta_g$) was evidenced by the appearance of the characteristic $^1O_2$ ($^1\Delta_g$) → $^3O_2$ phosphorescence at 1270 nm. Time resolved phosphorescence detection was used for singlet oxygen detection. The near IR luminescence of $^1O_2$ ($^1\Delta_g$) was observed at 90° geometry through a 5 mm thick antireflective coated silicon metal filter with a wavelength pass >1.1 μm and

dx.doi.org/10.1021/jp506890r | J. Phys. Chem. A 2014, 118, 9661−9674

an interference filter at 1.27 μm by means of a preamplified (low impedance) Ge-photodiode (Applied Detector Corporation, time resolution 1 μs). Simple exponential analysis of the emission decay was performed with the exclusion of the initial part of the signal. The quantum yield of $^1O_2$ ($^1\Delta_g$) formation, Φ_Δ, was determined by measuring its phosphorescence intensity using an optically matched solution of phenalenone ($\Phi_\Delta = 0.98$)[32] as a reference sensitizer.

Protonation Studies and Spectroscopic Analysis. pK_a values were determined by spectrophotometric pH titrations using NaH_2PO_4/Na_2HPO_4 (each 0.1 M) buffer. In each experiment, 50 mL of solution containing the Re(I) complex ([Re] = 3×10^{-5} M), initially at pH = 6.7, were turned to pH = 10.0 by addition of NaOH 3 M. After that, the pH was gradually lowered to pH = 2.0 by addition of 50 or 100 μL aliquots of $HClO_4$ 3 M, and then the absorption spectrum of each solution was recorded. The procedure was repeated reversing the pH from 2 to 10 by adding 50 to 100 μL aliquots of NaOH 3 M. When it was necessary, the absorbances were corrected by the appropriate dilution factors.

A bilinear regression analysis[33] was applied to the experimental absorption matrix in order to obtain information on the spectra of the absorbing species. These methods can be applied to bilinear spectroscopic data from a chemical reaction to provide information about composition changes in an evolving system. In the present work we used the alternating least-squares (ALS) algorithm to simultaneously estimate concentration and spectral profiles. ALS extracts useful information from the experimental data matrix $\boldsymbol{A}(i \times j)$ by the iterative application of the following matrix product: $\boldsymbol{A} = \boldsymbol{C}\boldsymbol{S}^T + \boldsymbol{E}$ where $\boldsymbol{C}(i \times n)$ is the matrix of the concentrations profiles; $\boldsymbol{S}^T(n \times j)$ is that containing the spectral profiles, and $\boldsymbol{E}(i \times j)$ represents the error matrix. The indexes i, n, and j denote the sampling pHs, absorbing species and recorded wavelengths, respectively.

Computational Methods. DFT and TD-DFT calculations of ground and excited state properties of different *fac*-ReX(CO)$_3$(α-diimine) complexes have been lately employed to shed light on the role played by MLCT, LLCT and IL electronic transitions in the absorption spectra of those Re(I) complexes.[34−43]

DFT calculations on the electronic structure of the complexes were carried out with Gaussian 09 software.[44−47] Ground state geometry optimization was performed with the B3LYP hybrid functional using the LanL2DZ basis set.[48−53] The calculation yielded positive vibrational frequencies which confirmed that the ground state structures were minima on the energy surfaces. The energies of the vertical electronic transitions were computed at the optimized geometry of the ground-state by TD-DFT[54−56] with the PBE0 hybrid functional. The following basis sets: 6-311G, 6-311G*, and LanL2TZ(f) (TZ, ECP + f polarization) were used in TD-DFT calculations for C, N, O, and H atoms, Cl and S atoms and Re atom, respectively.[57,58] Solvent effects (methanol or water) were included in both DFT and TD-DFT calculations by way of the polarizable continuum model.[59−61] The number of calculated singlet-to-singlet electronic transitions was 110. Output files from Gaussian 09 were analyzed with the AOMix program.[62,63] By this way, density-of-states (DOS) spectra and percentage compositions of different molecular fragments to molecular orbitals (MOs) were obtained. GaussSum 2.2.5 program was used to simulate absorption spectra with Gaussian distributions with a full-width at half-maximum (fwhm) set to 3000 cm^{-1}.

RESULTS AND DISCUSSION

Origins of the Absorption Spectroscopy of *fac*-XRe(CO)$_3$L Complexes. In the electronic spectrum of *fac*-XRe(CO)$_3$L complexes the lowest energy absorption bands appear in the near-UV region. Different electronic transitions, like ligand-field (LF), metal-to-ligand charge transfer (MLCT), ligand-to-ligand charge transfer (LLCT), and intraligand (IL), contribute to the near UV-spectroscopy of those Re(I) complexes. Generally, charge transfer (CT) bands, which are centered at $\lambda_{max} \sim 330-400$ nm and have extinction coefficients of $\varepsilon \sim (2-5) \times 10^3$ M^{-1} cm^{-1}, have rather longer λ_{max} than the more intense IL band, as the latter appears at $\lambda_{max} \sim 240-320$ nm and has $\varepsilon \sim 2 \times 10^4$ M^{-1} cm^{-1}.[1] The correctness of these basic models has recently been questioned by TD-DFT calculations. Since mixing usually occurs between MLCT/LLCT or MLCT/XLCT, those transitions are now called metal−ligand-to-ligand charge transfer (MLLCT) transitions. For instance, in complexes like [Re(bpy)(CO)$_3$Cl] and [Re(bpy)(CO)$_3$(py)]$^+$ (bpy = 2,2′-bipyridine, py = pyridine), the HOMO can be described as containing more than 50% of Re character, with contributions of around 20% each from CO and Cl in the case of [Re(bpy)(CO)$_3$Cl] and 20% from CO in [Re(bpy)(CO)$_3$(py)]$^+$. However, the LUMO is composed of more than 80% of bpy character in both cases.[2] Consequently, a MLLCT character can be ascribed to the lowest energy electronic transition. Furthermore, we have recently described examples of water-soluble Re(I) complexes with their lowest energy absorption bands of MLLCT character.[25,64] LLCT excited states are manifested in complexes that bear both reducing and oxidizing type of ligands. Consequently, a charge transfer occurs between the donor and the acceptor ligand. Several examples of *fac*-XRe(CO)$_3$L complexes with lowest excited states featuring a LLCT character have been reported.[2] As a consequence of the extremely weak donor−acceptor electronic interaction, those complexes usually display very low ε in their LLCT bands. A consequence of this is that, unlike to MLCT transitions, LLCT transitions are not usually observed directly from absorbance UV−vis spectroscopy. Since LLCT states are frequently nonluminescent, only transient spectroscopy can be useful to study their photophysical properties.[2] Because of the last observations, LLCT states are usually elusive when compared to MLCT states.

Absorption Spectroscopy of [ClRe(CO)$_3$(BCS)]$^{2-}$. The absorption spectrum of [ClRe(CO)$_3$(BCS)]$^{2-}$ in aqueous neutral solutions, i.e. at pH = 7.0, consists of a strong absorption band ($\varepsilon \sim 2 \times 10^4$ M^{-1} cm^{-1}) centered at λ_{max} = 296 nm with a shoulder at 333 nm. Between 350 and 400 nm, there is a rather flat portion of the spectrum, centered at 376 nm, consisting of at least of two bands of medium intensity ($\varepsilon \sim 3 \times 10^3$ M^{-1} cm^{-1}). When compared to the neutral solution, in acidic media (pH = 2.0) the spectrum hardly experiences any changes between 290 and 400 nm though there is an intensity enhancement in the 220−290 nm range. In alkaline media (pH = 10.0), however, the high energy band shifts to λ_{max} = 291 nm while the lowest energy bands, compared to the neutral solutions, shift to longer wavelengths. A reversible pH dependent ligand exchange is found in the UV−vis spectrum of the Re(I) complex in the pH = 2.0−10.0 range. We measured the UV−vis spectrum of [ClRe(CO)$_3$(BCS)]$^{2-}$ in NaH_2PO_4/Na_2HPO_4 buffer solutions at room temperature and

dx.doi.org/10.1021/jp506890r | J. Phys. Chem. A 2014, 118, 9661−9674

titrations were carried out by adding aqueous $HClO_4$ to observe spectral changes (see Figure 1a). Figure 1a can be split in two pH ranges: (i) the spectral changes observed between pH = 10 and pH = 7, where two isosbestic points at 255 and 345 nm can be discerned and (ii) the spectral changes observed between pH = 7 and pH = 2 where no isosbestic points are present. This behavior is indicative of the existence of various species in simultaneous equilibriums. Therefore, we decided to apply bilinear regression analysis techniques in the analysis of the full matrix of UV−vis spectra of Figure 1a to get an understanding of the pH influence on the corresponding equilibriums between the different species. The estimation of the number of independent contributions yielded $n = 3$. The inset to Figure 1a shows the distribution functions for the three species over the whole pH range. From this figure, there are two pH values at which each pair of species has the same concentration, i.e. 5.6 and 8.6. According to literature reports,[65,66] $[ClRe(CO)_3(BCS)]^{2-}$ may suffer hydrolysis in aqueous solutions to yield $[(H_2O)Re(CO)_3(BCS)]^-$. With a related water-soluble Re(I) complex, i.e., $Re(CO)_3$(pterin)-(H_2O), we previously found that deprotonation of water molecule to yield the hydroxo complex occurred with a pK_a of 8.8.[24] Consequently, the three species that should be considered contributing to the pH dependent spectral changes are $[ClRe(CO)_3(BCS)]^{2-}$, $[(OH)Re(CO)_3(BCS)]^{2-}$ and $[(H_2O)Re(CO)_3(BCS)]^-$. Therefore, pH = 8.6 can be ascribed to the equilibrium between $[ClRe(CO)_3(BCS)]^-$ and $[(HO)Re(CO)_3(BCS)]^{2-}$ species. Regarding the pH = 5.6, it could be ascribed to the replacement of Cl^- by H_2O in the coordination sphere of the Re(I) complex, eq 3-4.

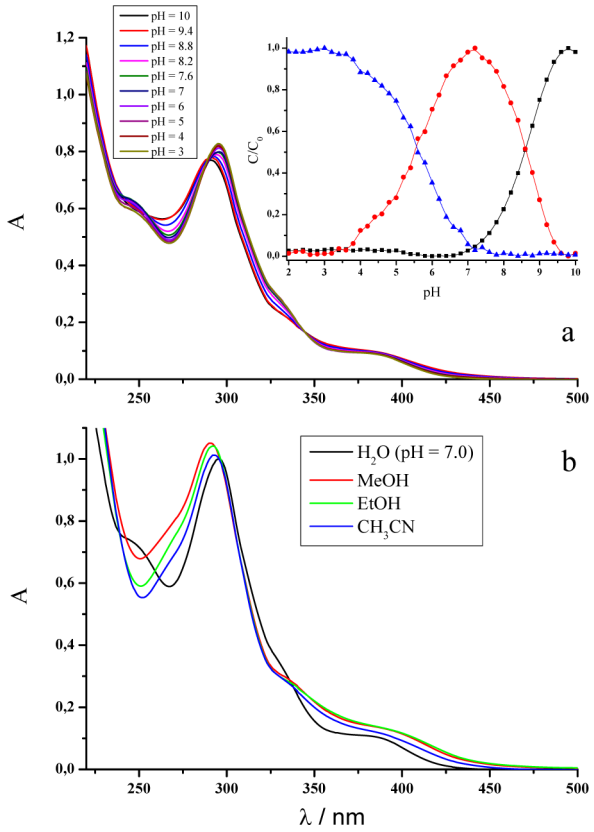

Figure 1. (a) UV−vis spectrum of $[ClRe(CO)_3(BCS)]^{2-}$ measured in buffer solutions at different pH values in the range 2.0−10.0. Inset: distribution functions for the three species obtained in the bilinear analysis of the absorption spectra in the whole pH range. (b) UV−vis absorption spectra of $[ClRe(CO)_3(BCS)]^{2-}$ in different solvents.

$$[ClRe(CO)_3(BCS)]^{2-} + H_2O \rightleftarrows [(H_2O)Re(CO)_3(BCS)]^- + Cl^- \quad (3)$$

$$[ClRe(CO)_3(BCS)]^{2-} + OH^- \rightleftarrows [(HO)Re(CO)_3(BCS)]^{2-} + Cl^- \quad (4)$$

Figure 1b shows a comparison of the UV−vis absorption spectra of $[ClRe(CO)_3(BCS)]^{2-}$ in water, acetonitrile, methanol, and ethanol solutions. It is observed that the high energy absorption band shifts from λ_{max} = 296 nm in water to λ_{max} = 291−293 nm in the organic solvents. Additionally, the low energy band broadens and shifts to longer wavelengths.

TD-DFT Calculations. TD-DFT calculations were performed on different geometry optimized structures corresponding to the existing species in organic or in aqueous solutions to better understand the solvent effects on the photophysical properties of the Re(I) complex. In the following section, TD-DFT results corresponding to the lowest energy band of the Re(I) complex will be discussed in detail, as the electronic transitions in this near UV−vis energy region are the ones responsible of the observed luminescence of the Re(I) complex (communicated in the Steady state and time-resolved luminescence section, see below).

TD-DFT calculations were performed on $[ClRe(CO)_3(BCS)]^{2-}$ (PCM/MeOH and PCM/H_2O) and $[(H_2O)Re(CO)_3(BCS)]^-$ (PCM/H_2O). Since TD-DFT results for $[ClRe(CO)_3(BCS)]^{2-}$ were very similar under the polarizable continuum model in H_2O and MeOH, only the TD-DFT calculated results for $[ClRe(CO)_3(BCS)]^{2-}$ (CPM/MeOH) and $[(H_2O)Re(CO)_3(BCS)]^-$ (CPM/H_2O) will be discussed. The calculated TD-DFT results are summarized and compared with experimental data in Table 1 for $[ClRe(CO)_3(BCS)]^{2-}$ (in MeOH) and $[(H_2O)Re(CO)_3(BCS)]^-$ (in H_2O). It is observed that the main spectral features are predicted to a great accuracy, both in position and relative intensities, by TD-DFT calculations. The main MOs involved in the most intense electronic transitions of $[ClRe(CO)_3(BCS)]^{2-}$ and $[(H_2O)Re(CO)_3(BCS)]^-$ in the 340−400 nm wavelength region (i.e., the spectral region corresponding to the excitation wavelengths used in the luminescence experiments described below) are H, H − 1, L, and L + 1. Figures 2 and 3 show spatial plots of those MOs for $[ClRe(CO)_3(BCS)]^{2-}$ and $[(H_2O)Re(CO)_3(BCS)]^-$, respectively. Spatially, L and L + 1 are very similar in shape for both $[ClRe(CO)_3(BCS)]^{2-}$ and $[(H_2O)Re(CO)_3(BCS)]^-$. The difference arises in the H. For $[ClRe(CO)_3(BCS)]^{2-}$, H is spatially limited to the vicinities of Re, Cl and the three carbonyls. For $[(H_2O)Re(CO)_3(BCS)]^-$, however, H is widespread through the whole molecule, including also distant sulfonates.

The corresponding molecular energy and wave function (ψ) are obtained from the calculation of an electronic structure of a given electronic state. As ψ depends on the coordinates of all the electrons, it is not very appropriate for interpretation. Hence, in order to get a deeper insight into the electronic structure of molecules, simplified notions and characteristics of ψ are required. The most widely used procedure to get information on the electronic structure of molecules is through the Mulliken population analysis (MPA). The AOMIX program

dx.doi.org/10.1021/jp506890r | J. Phys. Chem. A 2014, 118, 9661−9674

Table 1. Comparison of experimental absorption data of the Re(I) complex in MeOH and H_2O with TD-DFT calculations for $[ClRe(CO)_3(BCS)]^{2-}$/PCM/MeOH and $[(H_2O)Re(CO)_3(BCS)]^{-}$/PCM/$H_2O$, respectively. Electronic transitions are computed at the PBE0-CPM/LanL2TZ(f)/6-311G/6-311G* level of theory

solvent	λ_{obs}/nm ($\varepsilon/10^3$ $M^{-1}cm^{-1}$)	λ_{calc}/nm (f_{osc})	major contributions to the electronic transitions (% coefficients)
MeOH	385 (4.9)	390.9 (0.112)	H − 1 → L (92%)
		358.2 (0.1223)	H → L + 1 (85%)
		346.0 (0.1617)	H − 1 → L + 1 (95%)
	329 (11.2)	330.3 (0.0644)	H − 7 → L (15%), H − 5 → L (69%)
		325.4 (0.1344)	H − 2 → L + 1 (93%)
		300.7 (0.2059)	H − 7 → L (35%), H − 6 → L + 1 (21%), H − 5 → L (14%)
	291 (37.8)	294.1 (0.4402)	H − 8 → L (67%), H − 5 → L + 1 (11%)
		285.9 (0.1676)	H − 8 → L + 1 (10%), H − 7 → L (28%), H − 6 → L + 1 (41%)
		273.2 (0.0577)	H − 8 → L + 1 (40%)
		272.8 (0.0797)	H − 15 → L (60%)
	263 (27.0)	263.5 (0.1688)	H → L + 2 (30%), H → L + 4 (28%), H → L + 8 (11%)
		252.2 (0.0569)	H − 18 → L (62%)
		233.2 (0.0724)	H − 19 → L (15%), H − 6 → L + 2 (15%), H → L + 11 (15%), H → L + 14 (12%)
		232.3 (0.1012)	H − 23 → L (16%), H − 1 → L + 8 (20%), H − 1 → L + 11 (18%), H − 1 → L + 14 (10%)
		232.1 (0.071)	H − 21 → L (21%), H − 6 → L + 2 (15%), H − 3 → L + 2 (13%)
		231.9 (0.0524)	H − 22 → L (13%), H − 21 → L (31%)
		231.7 (0.0522)	H − 22 → L (40%), H − 4 → L + 2 (14%)
		227.8 (0.0536)	H − 6 → L + 3 (13%), H → L + 7 (28%)
		224.9 (0.0735)	H − 7 → L + 4 (13%), H − 6 → L + 3 (26%), H − 5 → L + 4 (12%)
water	378 (5.2)	385.7 (0.1943)	H → L (92%)
		337.2 (0.2897)	H → L + 1 (89%)
	324 (17.5)	320.9 (0.2831)	H − 5 → L (21%), H − 3 → L + 1 (36%), H − 1 → L + 1 (33%)
		312.3 (0.067)	H − 6 → L (76%)
		297.1 (0.1105)	H − 10 → L (33%), H − 8 → L (22%), H − 7 → L + 1 (16%)
	295 (44.6)	293.4 (0.1468)	H − 3 → L + 2 (10%), H − 1 → L + 2 (10%), H → L + 3 (22%), H → L + 5 (12%)
		291.1 (0.2785)	H − 7 → L + 1 (13%), H − 5 → L + 1 (49%)
		283.5 (0.076)	H − 6 → L + 1 (64%)
	250 (32.0)	259.2 (0.0669)	H − 15 → L (69%)
		249.1 (0.1093)	H − 3 → L + 4 (16%), H − 1 → L + 4 (18%), H → L + 3 (15%), H → L + 5 (20%)
		246.0 (0.0882)	H − 13 → L + 1 (17%), H − 3 → L + 4 (13%), H → L + 3 (12%), H → L + 5 (20%)
		234.9 (0.0608)	H - 4 → L + 9 (14%), H − 3 → L + 11 (21%), H − 1 → L + 11 (19%)
		234.0 (0.1626)	H − 3 → L + 5 (17%), H − 1 → L + 5 (15%), H → L + 6 (13%)
		230.4 (0.0924)	H − 6 → L + 2 (52%), H − 6 → L + 4 (15%)
		226.1 (0.0832)	H − 6 → L + 3 (11%), H − 6 → L + 5 (10%), H − 5 → L + 4 (20%)
		225.4 (0.0759)	H − 4 → L + 3 (13%), H − 4 → L + 5 (11%), H → L + 9 (10%)
		218.9 (0.0511)	H − 7 → L + 4 (12%), H − 6 → L + 3 (22%), H − 6 → L + 5 (10%)
		216.8 (0.0663)	H − 10 → L + 2 (10%), H − 6 → L + 4 (15%), H − 5 → L + 3 (10%)
		210.8 (0.0639)	H − 10 → L + 3 (17%), H − 6 → L + 5 (23%)

uses MPA to calculate, for example, DOS.[64] A pictorial representation of MO compositions can be obtained from plots of DOS spectra based on the contributions of the different fragments in which the whole molecule can be split for analysis. Figure 4 shows DOS spectra for $[ClRe(CO)_3(BCS)]^{2-}$ and $[(H_2O)Re(CO)_3(BCS)]^{-}$. The DOS spectra were generated from contributions of six fragments: (i) Re atom, (ii) the three carbonyls, (iii) Cl atom or H_2O molecule, (iv) $(CH_3)_2$–phenanthroline, (v) the two phenyl groups, and (vi) the two sulfonates. Table 2 lists the orbital percentage composition of the relevant MOs of $[ClRe(CO)_3(BCS)]^{2-}$ and $[(H_2O)Re(CO)_3(BCS)]^{-}$calculated with the AOMIX program.

In MeOH, the lowest energy band of $[ClRe(CO)_3(BCS)]^{2-}$, which is observed at around 385 nm, is predicted by TD-DFT at 390.9 nm as a H − 1 → L transition. Given the orbital percentage composition of H − 1 and L (Table 2), H − 1 → L transition is composed of two kind of electronic transitions. One of them is a $MLLCT_{ClRe(CO)_3\rightarrow BCS}$ transition (i.e., a delocalized $ClRe(CO)_3$ → BCS CT transition) with most of the electron density transferred from the Re−C and Re−Cl bonds to the $(CH_3)_2$-phenanthroline fragment of BCS. The other transition is an IL transition involving charge density transferred from the sulfonates to the phenyl fragments of BCS. Transition H − 1 → L + 1, which is predicted at 346.0 nm, is very similar in nature to the electronic transition H − 1 → L. The only difference arises in the higher percentage contribution of the phenyl groups and the lower contributions of Re and Cl fragments in L + 1 than in L. The electronic transition predicted at 358.2 nm is a H → L + 1 transition. Since the Re atom contribute with higher percentages to H than to H − 1, the H → L + 1 transition has higher charge transfer character than H − 1 → L and H − 1 → L + 1 electronic transitions. For characterization of the electronic transitions as partial CT transitions, the following definition of the CT character can be used, eq 5:[67]

$$CT_I\ (\%) = 100(P_g(M) - P_I(M)) \quad (5)$$

dx.doi.org/10.1021/jp506890r | J. Phys. Chem. A 2014, 118, 9661−9674

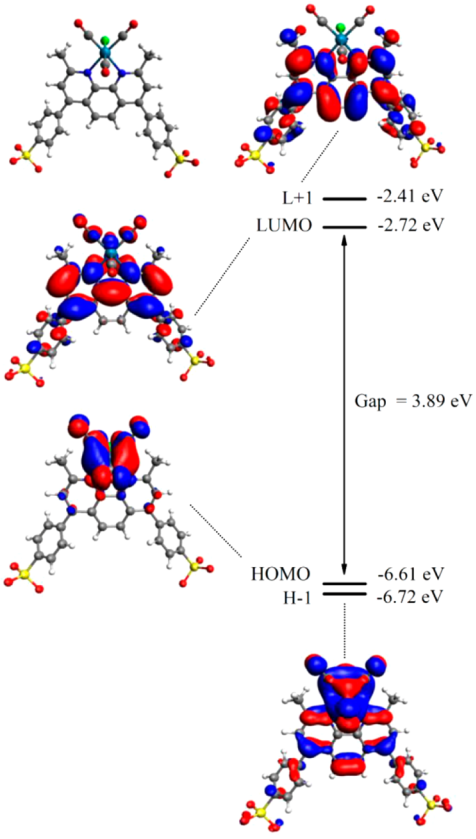

Figure 2. Frontier orbital diagram for $[ClRe(CO)_3(BCS)]^{2-}$/PCM/MeOH (isovalue =0.02). H − 1 → L, H − 1 → L + 1 and H → L + 1 are the main transitions involved in the low energy absorption band of the complex in MeOH. Optimized geometries and TD-DFT calculations were carried out including solvent effects through the polarizable continuum model (PCM). See text for details.

In this equation, $P_g(M)$ and $P_I(M)$ represent the metal electronic density in the ground state and the *I*-th excited state, respectively. MLCT transitions correspond to positive $CT_I(M)$ values while negative $CT_I(M)$ values correspond to LMCT transitions.[67]

For a H − *n* → L + *m* excitation, the CT character becomes

$$CT\ (\%) = \%(Re)_{H-n} - \%(Re)_{L+m} \quad (6)$$

If the excited state is formed by more than one one-electron excitation, then the metal CT character of this excited state is expressed in eq 7 as a sum of CT characters of each participating excitation, $i \rightarrow j$.[67]

$$CT_I(\%) = \sum_i [C_I(i \rightarrow j)]^2[\%(M)_i - \%(M)_j] \quad (7)$$

where $C_I(i \rightarrow j)$ are the appropriate coefficients of the *I*th transition giving the percentage contribution of a configuration to the resulting excited state TD-DFT wave function. Therefore, with the aid of eqs 4−6 and the orbital percentages of Table 2, for $[ClRe(CO)_3(BCS)]^{2-}$, a 47% of CT can be calculated for H → L + 1 transition. On the other hand, H − 1 → L and H − 1 → L + 1 electronic transitions have 37 and 38% of CT, respectively.

For the $[(H_2O)Re(CO)_3(BCS)]^-$ complex, in H_2O, TD-DFT predicts two low energy electronic transitions in the 340−390 nm spectral region: a H → L transition at 385.6 nm and a H → L + 1 transition at 337.2 nm. Both can be described as

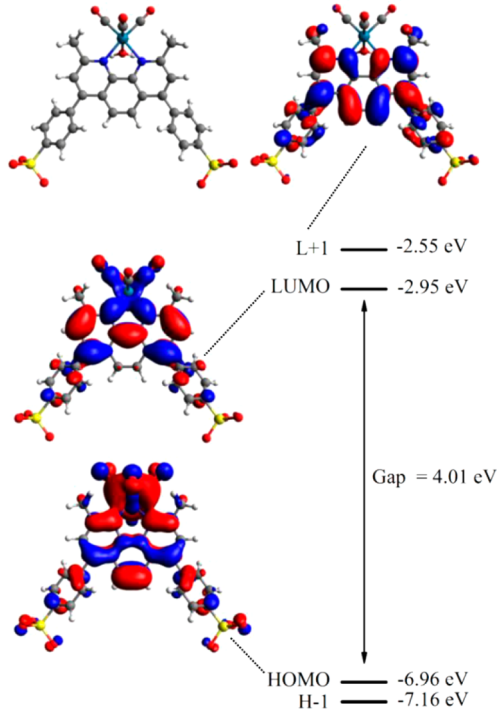

Figure 3. Frontier orbital diagram for $[(H_2O)Re(CO)_3(BCS)]^-$/PCM/H_2O (isovalue =0.02). H → L and H → L + 1 are the main transitions involved in the low energy absorption band of the complex in aqueous solutions. Optimized geometries and TD-DFT calculations were carried out including solvent effects through the polarizable continuum model (PCM). See text for details.

admixtures of MLLCT and IL electronic transitions. For H → L and H → L + 1 transitions, 25 and 27% of CT can be calculated, respectively. Therefore, the balance between MLLCT and IL is inclined toward the latter and the IL states seem to play a predominant role in the photophysical processes in aqueous solutions. To ease the comparison with experimental data, TD-DFT calculated electronic transitions were used to simulate the absorption spectra of $[ClRe(CO)_3(BCS)]^{2-}$ and $[(H_2O)Re(CO)_3(BCS)]^-$ with the aid of eq 8[68] by summing Gaussian functions centered at each calculated wavelength with the maxima related to the value of the oscillator strengths (f_{osc})

$$\varepsilon(\tilde{\upsilon}) = \frac{2.175 \times 10^8\ L\ mol^{-1}\ cm^{-2}}{\Delta_{1/2}\tilde{\upsilon}}(f_{osc}) \exp\left[-2.772\left(\frac{\tilde{\upsilon} - \tilde{\upsilon}_{i\rightarrow f}}{\Delta_{1/2}\tilde{\upsilon}}\right)^2\right] \quad (8)$$

where $\Delta_{1/2}\tilde{\upsilon}$ and $\tilde{\upsilon}_{i\rightarrow f}$ (both in units of cm^{-1}) are the parametrical value of the fwhm of the band and the frequency corresponding to the wavelength of the calculated electronic transition, respectively. Figure 5 shows the simulations and the values of f_{osc} in comparison with the experimental absorptions. The simulated spectra follow the observed absorptions with great accuracy both in position and relative intensities showing that the comparison is quite satisfactory.

Steady State and Time-Resolved Luminescence. The steady state luminescence of $[ClRe(CO)_3(BCS)]^{2-}$ shows a strong solvent and excitation wavelength dependence. Figure 6 shows the emission spectrum of N_2-deaerated solutions of the

dx.doi.org/10.1021/jp506890r | J. Phys. Chem. A 2014, 118, 9661−9674

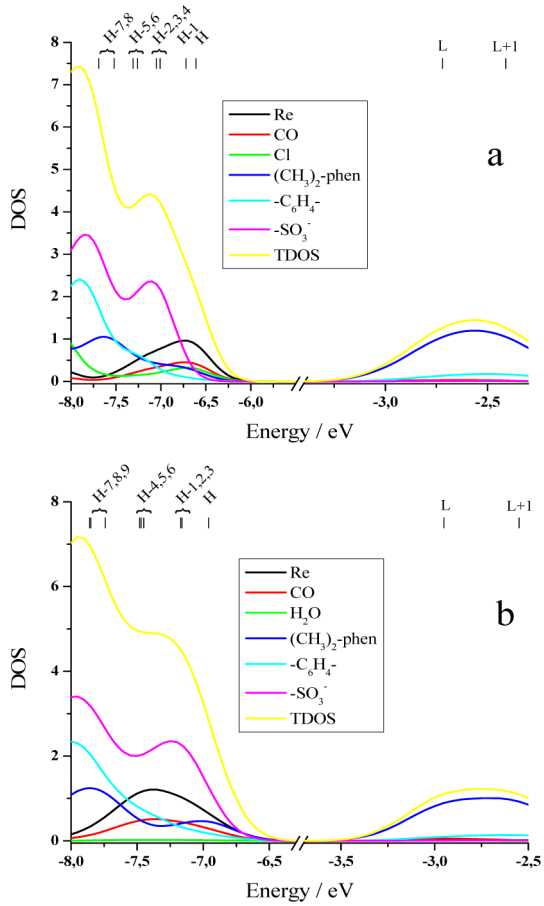

Figure 4. Total density of states (TDOS) and partial density of states (DOS) plots for (a) $[ClRe(CO)_3(BCS)]^{2-}$/PCM/MeOH and (b) $[(H_2O)Re(CO)_3(BCS)]^{-}$/PCM/$H_2O$ generated from contributions of six fragments: (i) Re atom, (ii) the three carbonyls, (iii) Cl atom, or H_2O molecule, (iv) $(CH_3)_2$–phenanthroline, (v) the two phenyl groups and (vi) the two sulfonates. The lines mark the position in energy of the different MOs. Optimized geometries and TD-DFT calculations were carried out including solvent effects through the polarizable continuum model (PCM). See text for details.

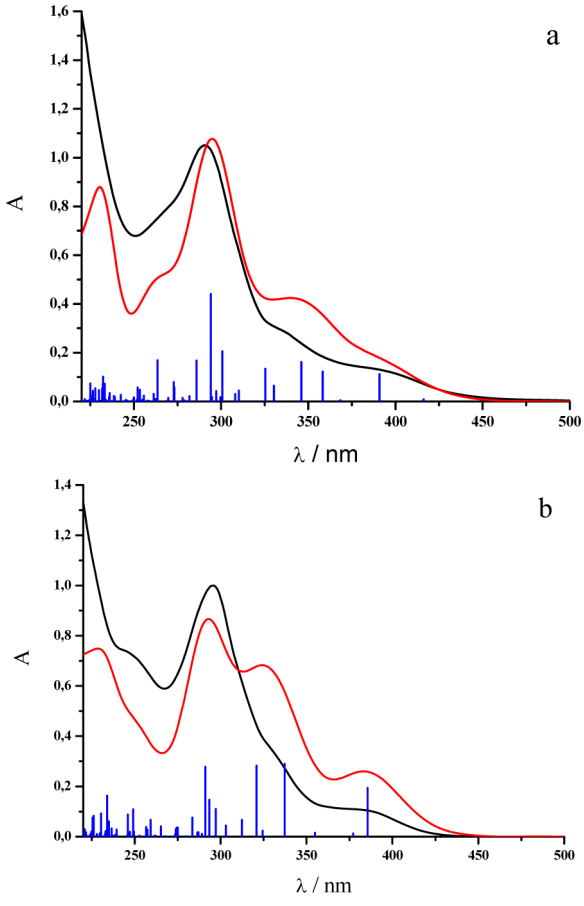

Figure 5. Comparison of the UV–vis absorption spectrum (black lines) with TD-DFT calculated electronic transitions (blue lines) and simulated spectra (red lines) for (a) $[ClRe(CO)_3(BCS)]^{2-}$/PCM/MeOH and (b) $[(H_2O)Re(CO)_3(BCS)]^{-}$/PCM/$H_2O$.

Re(I) complex in H_2O, CH_3CN, MeOH and EtOH with λ_{exc} = 350 and 400 nm. When the spectrum was taken in water, λ_{exc} = 350 nm, the emission occurred peaking at λ_{max} = 451 nm, with a shoulder at longer wavelengths centered around 570 nm. In the same solvent, however, when the excitation wavelength was 400 nm, the main emission peaked at 577 nm and only vestiges of the high energy band centered at 451 nm can be observed. In CH_3CN, EtOH, and MeOH, with λ_{exc} = 350 nm, the maximum of the luminescence spectrum occurred at 576, 590, and 595 nm, respectively. When the excitation wavelength was 400 nm, the emission peaked at 585, 591, and 590 nm in CH_3CN, EtOH, and MeOH, respectively (not shown).

A sum of two exponentials were required to achieve a satisfactory fit of the emission decay profiles of the O_2-free Re(I) complex solutions in the organic solvents. A fast component decay, $\tau_{short} \approx 5$ ns, was nearly independent of the solvent. However, the slow component decay lifetime, τ_{long}, was 148, 131, and 95 ns in CH_3CN, EtOH and MeOH, respectively. The presence of O_2 in the solutions quenched both the steady state and time-resolved luminescence of the Re(I) complex in the organic solvents. For instance, in MeOH, τ_{long} = 63.0 ns in air equilibrated solutions while τ_{long} = 30 ns in O_2 equilibrated solutions. A similar decrease of τ_{long} with the

Table 2. Composition (% character) of relevant Molecular Orbitals of $[ClRe(CO)_3(BCS)]^{2-}$ and $[(H_2O)Re(CO)_3(BCS)]^{-}$ calculated with the AOMIX program. MO energies are computed at the PBE0-CPM/LanL2TZ(f)/6-311G/6-311G* level of theory

compound	MO (energy/eV)	Re	CO	Cl/H_2O	$(CH_3)_2$–phen	phenyls	sulfonates
$[ClRe(CO)_3(BCS)]^{2-}$	H − 1 (−6.72)	40.3	18.5	14.0	19.9	5.8	1.5
	HOMO (−6.61)	50.4	24.4	18.5	5.0	1.4	0.3
	LUMO (−2.72)	3.3	3.4	1.0	82.5	9.2	0.6
	L + 1 (−2.41)	0.3	0.8	0.0	83.3	14.6	1.1
$[(H_2O)Re(CO)_3(BCS)]^{-}$	HOMO (−6.96)	31.0	14.7	1.3	39.0	10.5	3.5
	LUMO (−2.95)	4.6	5.7	0.8	80.3	8.1	0.6
	L + 1 (−2.55)	0.4	0.8	0.0	85.0	12.9	0.9

dx.doi.org/10.1021/jp506890r | J. Phys. Chem. A 2014, 118, 9661–9674

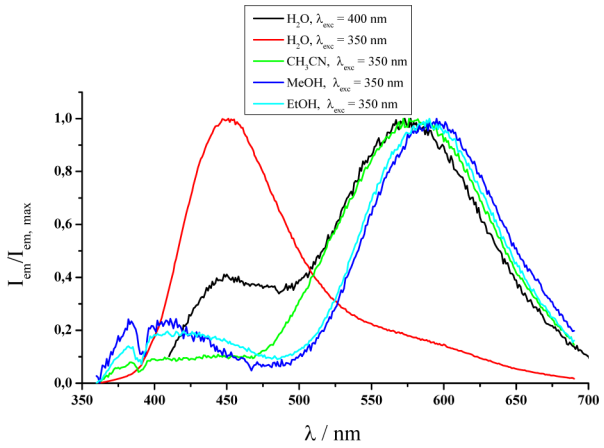

Figure 6. Solvent and excitation wavelength dependence of $[ClRe(CO)_3(BCS)]^{2-}$ emission spectrum. Solutions were deaerated by bubbling N_2.

increase of O_2 concentration was observed in CH_3CN and/or EtOH solutions, see Table 3.

The effect of pH on the luminescence of the Re(I) complex was studied in air equilibrated NaH_2PO_4/Na_2HPO_4 buffer solutions between pH = 2.0 and pH = 10.0 under similar experimental conditions to those used to investigate the effect of pH upon UV–vis absorption spectra (see Figure 7a). In the pH range between 10.0 and 7.5, the luminescence spectrum shows two band maxima centered at 410 and 570 nm and the luminescence quantum yield remains nearly constant, i.e. $\Phi_{em} \approx 0.012$. Decreasing the pH of the solution from 7.0 to 2.0 produces a dramatic increase in the luminescence quantum yield (by nearly a 6-fold, see inset to Figure 7a) as well as a bathochromic shift of the emission maximum from 410 to 451 nm. The emission centered at 570 nm, which was evident at pH < 7, is still present as a shoulder in the long wavelength tail of the luminescence. When the same experiment was carried out in the presence of NaCl 0.1 M, the decrease of the pH of the solution from 7.0 to 2.0 produced an increase in the luminescence quantum yield by only a factor of 2 (Spectra not shown).

In air equilibrated aqueous solutions, when the luminescence decays were monitored at λ_{em} = 451 nm, τ_{short} and τ_{long} were pH dependent. Between pH = 2.0 and pH = 7.0, $\tau_{long} \approx 7$ ns and then it was observed to decrease to $\tau_{long} \approx 4$ ns at pH = 10.0. Nevertheless, the fast component decay remains constant between pH = 2.0 and pH = 5.5 ($\tau_{short} \approx 2.2$ ns), then it reaches a maximum value of 3.0 ns at pH = 7.0, and afterward it decreases monotonically to $\tau_{short} \approx 1.1$–1.3 ns at higher pHs, see Table 4. Those lifetimes were nearly independent of O_2 concentration. For instance, τ_{short} = 2.9, 3.0, and 2.6 ns and τ_{long} = 6.6, 6.5, and 6.0 ns in N_2, air and O_2 equilibrated pH = 7.0 solutions, respectively. However, when the luminescence

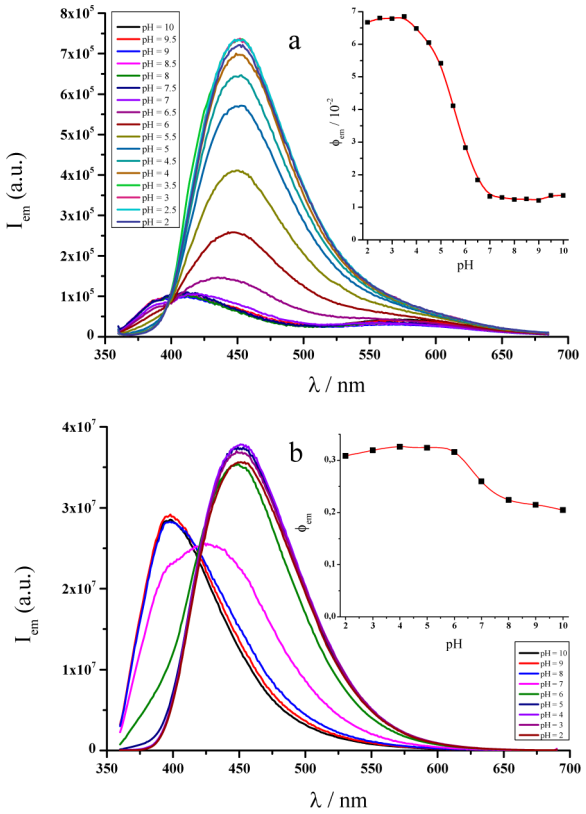

Figure 7. pH dependence of the emission spectrum (λ_{exc} = 350 nm) for air equilibrated solutions of: (a) the Re(I) complex and (b) BCS. Each inset shows the pH dependence of the corresponding emission quantum yield. See text for details.

decays were monitored at λ_{em} = 570 nm, τ_{short} and τ_{long}, in N_2-deaerated solutions, were 10 and 105 ns, respectively, with a decrease of τ_{long} with the increase of O_2 concentration, see Table 3.

A similar study of the pH effect on the luminescence of BCS was conducted for comparative purposes. Like other 2,9-aryl-substituted 1,10-phenanthrolines,[69] the BCS ligand experiences a single protonation event on N1–N10 with pK_a = 5.7–5.8.[70] The protonation of sulfonates in BCS is not expected at pH > 2.7.[70] The nonprotonated form of BCS displays a luminescence centered at 398 nm (see Figure 7b). After protonation, there is a bathochromic shift of the emission maximum to 451 nm with an increase in the luminescence quantum yield from Φ_{em} = 0.20 at pH = 10.0 to Φ_{em} = 0.33 at pH = 4.0 (see inset to Figure 7b). The luminescence lifetimes of BCS are 6.5 and 14.0 ns at pH = 4.0, and 3.5 ns at pH = 9.0. The acid–base behavior of the luminescence of BCS is consistent with the protonation/deprotonation effect on the luminescence of 2,9-aryl-substituted 1,10-phenanthrolines.[69] Indeed, 2,9-aryl-substituted

Table 3. Re(I) Complex Luminescence Lifetimes (λ_{exc} = 341 nm, λ_{ob} = 570 nm), Quantum Yields, and Bimolecular Rate Constants (k_q) for the Quenching of the Emission by Molecular Oxygen, in the Organic Solvents, and in Aqueous Buffer Solutions (pH = 7.0)

solvent	$\tau_{short}(N_2)$/ns	$\tau_{long}(N_2)$/ns	τ_{short}(air)/ns	τ_{long}(air)/ns	$\tau_{short}(O_2)$/ns	$\tau_{long}(O_2)$/ns	$k_q/10^9$ M^{-1} s^{-1}	Φ_{em}(air) (±10%)
MeOH	7 ± 2	95 ± 8	7 ± 2	63 ± 2	5 ± 1	30 ± 2	2.2 ± 0.1	8.8×10^{-3}
EtOH	4.6 ± 0.1	131 ± 2	4.5 ± 0.6	81 ± 4	3.9 ± 0.1	33.7 ± 0.4	2.20 ± 0.05	1.3×10^{-2}
CH_3CN	5 ± 1	148 ± 11	8 ± 2	80 ± 11	8 ± 2	35 ± 1	2.4 ± 0.1	2.6×10^{-2}
H_2O	10 ± 2	105 ± 10	8 ± 2	96 ± 10	9 ± 2	71 ± 7	3.7 ± 0.1	1.3×10^{-2}

dx.doi.org/10.1021/jp506890r | J. Phys. Chem. A 2014, 118, 9661–9674

Table 4. Re(I) Complex Luminescence Lifetimes (λ_{exc} = 341 nm, λ_{ob} = 451 nm) and Quantum Yields in the Aqueous Buffer Air-Saturated Solutions at Different pHs[a]

pH	τ_{short}/ns (±25%)	τ_{long}/ns (±5%)	Φ_{em} (±10%)	Φ_{em}(Sp1) (±20%)	Φ_{em}(Sp2) (±20%)	Φ_{em}(Sp3) (±20%)
2.0	2.2	7.1	6.7×10^{-2}	$<1 \times 10^{-4}$	6.2×10^{-2}	4.9×10^{-3}
2.5	2.2	7.0	6.8×10^{-2}	2.3×10^{-4}	6.3×10^{-2}	4.7×10^{-3}
3.0	2.1	7.0	6.7×10^{-2}	2.5×10^{-4}	6.2×10^{-2}	4.6×10^{-3}
3.5	2.3	7.0	6.8×10^{-2}	4.1×10^{-4}	6.3×10^{-2}	4.7×10^{-3}
4.0	2.3	7.1	6.3×10^{-2}	5.3×10^{-4}	5.8×10^{-2}	4.4×10^{-3}
4.5	1.9	7.0	5.8×10^{-2}	1.1×10^{-3}	5.2×10^{-2}	4.5×10^{-3}
5.0	2.4	7.0	5.3×10^{-2}	1.7×10^{-3}	4.7×10^{-2}	4.6×10^{-3}
5.5	2.2	7.0	3.9×10^{-2}	3.3×10^{-3}	3.1×10^{-2}	4.6×10^{-3}
6.0	2.7	7.0	2.8×10^{-2}	5.4×10^{-3}	1.8×10^{-2}	4.4×10^{-3}
6.5	2.9	6.9	1.8×10^{-2}	6.8×10^{-3}	7.3×10^{-3}	3.9×10^{-3}
7.0	3.0	6.5	1.3×10^{-2}	7.8×10^{-3}	1.8×10^{-3}	3.4×10^{-3}
7.5	2.5	5.0	1.3×10^{-2}	9.1×10^{-3}	$<1 \times 10^{-4}$	3.9×10^{-3}
8.0	2.6	4.7	1.2×10^{-2}	8.5×10^{-3}	$<1 \times 10^{-4}$	3.5×10^{-3}
8.5	1.9	4.2	1.2×10^{-2}	8.6×10^{-3}	$<1 \times 10^{-4}$	3.4×10^{-3}
9.0	1.3	3.9	1.1×10^{-2}	7.9×10^{-3}	$<1 \times 10^{-4}$	3.0×10^{-3}
9.5	1.1	3.8	1.2×10^{-2}	7.9×10^{-3}	$<1 \times 10^{-4}$	4.0×10^{-3}
10.0	1.4	3.9	1.2×10^{-2}	7.7×10^{-3}	$<1 \times 10^{-4}$	4.3×10^{-3}

[a]See text for details.

1,10-phenanthrolines fluorescence is of $^1\pi\pi^*$ character, with emission maxima, fluorescence lifetime, and fluorescence quantum yields in dichloromethane between $\lambda_{max} \approx 374$ and 408 nm, $\tau \approx 1.2$ and 2 ns and $\Phi_{em} \approx 0.08$ and 0.33, respectively. On the other hand, protonated 2,9-aryl-substituted 1,10-phenanthrolines show emission maxima, fluorescence lifetime, and fluorescence quantum yields in dichloromethane between $\lambda_{max} \approx 474$ and 600 nm, $\tau \approx 3.3$ and 8.7 ns and $\Phi_{em} \approx 0.01$ and 0.50, respectively.[69]

We applied bilinear regression analysis techniques in the study of the full matrix of luminescence spectra of Figure 7, parts a and b. For BCS, the estimation of the number of independent contributions yielded $n = 2$. Figure 8a shows the luminescence spectra of the two emitting species with the corresponding distribution functions for BCS. From those distribution functions a pK_a corresponding to the protonation/deprotonation of the excited state, i.e. pK_a* = 6.6, can be obtained. Therefore, the $^1\pi\pi^*$ excited state of BCS is less basic than the ground state by nearly 1 order of magnitude of K_a. On the other hand, the estimation of the number of independent species which contribute to the spectral changes of Figure 7a yielded $n = 3$. Figure 8b shows the spectral profiles of the three emitting species with the corresponding distribution functions for the Re(I) complex. After comparison of Figure 8, parts a and b, it can be concluded that the spectra in both figures corresponding to the species Sp2 are nearly the same while the ones corresponding to the species Sp1 are very similar. In Figure 8b, Sp1 prevails at pH between 10.0 and 7.0 while Sp2 is more abundant at pH < 6.0. Moreover, the spectrum which corresponds to the specie Sp3 in Figure 8b is very similar to the luminescence spectra of the Re(I) complex in aqueous solutions after excitation with λ_{exc} = 400 nm (Figure 6). This species emits in the whole pH range.

Table 4 shows also the pH dependence of the luminescence quantum yield of each species (i.e., Φ_{em}(Sp1), Φ_{em}(Sp2) and Φ_{em}(Sp3)) calculated from the total luminescence quantum yield (Φ_{em}, Table 4) and the distributions functions of Figure 8b.

Photophysical Processes of the Re(I) complex. Equations 9−11 summarize the series of events occurring

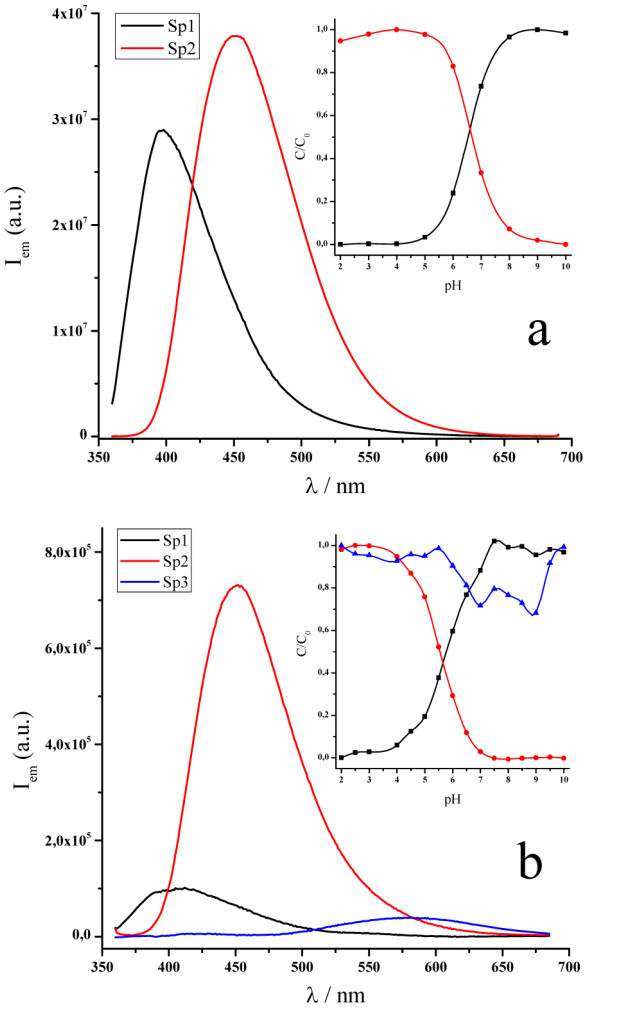

Figure 8. Spectral shapes for the different species and their distribution functions obtained from bilinear regression analysis of pH dependent emission spectral changes experienced by (a) BCS and (b) the Re(I) complex (see Figure 7). See text for details.

dx.doi.org/10.1021/jp506890r | J. Phys. Chem. A 2014, 118, 9661−9674

after optical excitation of $XRe(CO)_3L$ complexes with photonic energies ≤340 kJ/mol. In this energy region ^{1}IL states are usually not populated. ^{3}MLCT is generated by intersystem crossing (ISC) from the first excited singlet state (^{1}MLCT) in a few hundred femtoseconds.[1] Equations 10 and 11 represent the ^{3}MLCT exited state decay by monomolecular radiative and nonradiative processes.

$$[XRe(CO)_3L] \xrightarrow{h\upsilon} {}^1\text{MLCT} \xrightarrow{k_{isc}} {}^3\text{MLCT} \quad (9)$$

$${}^3\text{MLCT} \xrightarrow{k_r} [XRe(CO)_3L] + h\upsilon_{em} \quad (10)$$

$${}^3\text{MLCT} \xrightarrow{k_{nr}} [XRe(CO)_3L] \quad (11)$$

Equations 9−11 reflect the photophysical behavior of $XRe(CO)_3L$ complexes with L= bpy or phen and X=CF_3SO_3 and/or py, since nor bpy, phen, py or CF_3SO_3 have significant ^{1}IL states at energies ≤340 kJ/mol ($\lambda_{exc} \geq 350$ nm). However, when the ^{1}IL states have significant absorptions at the photonic energies used, their population have also to be considered, eq 12:

$$[XRe(CO)_3L] \xrightarrow{h\upsilon} {}^1\text{IL} \xrightarrow{k_{isc}} {}^3\text{IL} \quad (12)$$

By comparison with previous studies,[2] the luminescence of the $[ClRe(CO)_3(BCS)]^{2-}$ complex in organic solvents can be attributed to the ^{3}MLLCT. Moreover, the triplet character of the emitting excited state is manifested in the intrinsic quenching effect by O_2 in organic solvents. The values of the emission lifetimes in the absence and in the presence of oxygen (τ_0 and τ, respectively) were used to determine the bimolecular rate constants of the quenching of $[ClRe(CO)_3(BCS)]^{2-}$ emission by oxygen (k_q, Table 3) from the slopes of the linear Stern−Volmer plots ($\tau_0/\tau = 1 + k_q\tau_0[O_2]$). The saturated oxygen solubility at 1.013 bar O_2 partial pressure in the organic solvents and water, $[O_2]_{P=1,}$ were taken from literature values[28,72] to calculate the oxygen solubility at 1.013 bar of air according to $[O_2] = 0.21(P_A - P_v)[O_2]_{P=1}$,[71] where P_A and P_v are the atmospheric pressure and the vapor pressure of the solvent, respectively. The values of k_q obtained for the three organic solvents are between 2.2 and 2.4 × 10^9 M^{-1} s^{-1} while k_q = 3.7 × 10^9 M^{-1} s^{-1} in H_2O, see Table 3. They are in good agreement with k_q values reported for similar Re(I) complexes.[13,37]

On the other hand, luminescence experiments carried out in aqueous media are only compatible with the presence of both ^{1}IL and ^{3}MLLCT emitting species. Indeed, the effect of pH on the luminescence of the Re(I) complex can be explained on the basis of the coexistence of (i) a ^{3}MLLCT excited state (corresponding to Sp3 in Figure 8b) which follows a moderate dependence of Φ_{em} vs pH and (ii) two forms of coordinated BCS (Sp2/Sp1 species in Figure 8a) with a Φ_{em} strongly pH-dependent. These two forms of coordinated BCS show a sigmoid dependence of Φ_{em} vs pH (similar to the pH dependence of Φ_{em} of the ligand BCS, compare insets to Figures 7a and 7b), with a ratio of $\Phi_{em,(pH=2)}/\Phi_{em,(pH=10)} \approx 5.6$. However, the ratio of $\Phi_{em,(pH=2)}/\Phi_{em,(pH=10)}$ for the free BCS ligand is only 1.5. The enhancement of Φ_{em} of the Re(I) complex as pH decreases can be rationalized in terms of the equilibriums of eqs 3 and 4. In a pH range between 10.0 and 7.0, both $[ClRe(CO)_3(BCS)]^{2-}$ and $[(OH)Re(CO)_3(BCS)]^{2-}$ species are in a pH dependent equilibrium. Therefore, the charge density over the Re center should be nearly invariant, and the coordinated BCS may experience a small and approximately constant positive charge, $\delta+$. In this pH range Φ_{em} is nearly invariant. Note also that the emission spectrum of Sp1 in Figure 8b is more similar to the spectrum of BCS at pH = 7.0 than to the spectrum of BCS at pH = 10.0 (compare Figures 7b and 8b). At pH = 7.0, the protonated and bare forms of BCS in the excited state have similar concentrations (remember that pK_a^* = 6.6 for BCS). This suggests that in the Re(I) complex over the 10−7 pH range, the coordinated BCS ligand might be experiencing a $\delta+ \approx +^1/_2e$ (e = electron charge). In the pH range between 7.0 and 2.0, the replacement of Cl^- by H_2O in the coordination sphere of the Re(I) complex enhances the formal charge of the Re(I) center to $\delta+ \approx +1e$, with a consequent enhancement of Φ_{em}. It is to noteworthy that when the equilibrium of eq 3 was displaced to the left by performing the pH-dependent experiment on the luminescence of the Re(I) complex in the presence of an excess of NaCl, $\Phi_{em,(pH=2)}/\Phi_{em,(pH=10)}$ was only 2, in contrast to the value of $\Phi_{em,(pH=2)}/\Phi_{em,(pH=10)}$ = 5.6 which is observed in the absence of NaCl. The latter experiment clearly demonstrated that, when the concentration of Re(I) complexes bearing Cl^- species was enhanced, and thus mean $\delta+$ over the coordinated BCS is reduced, the ^{1}IL emission peaking at 410 nm is favored against the one centered at 451 nm.

The solvent dependent balance between ^{1}IL and ^{3}MLLCT excited states, which tune the photophysical properties of the Re(I) complex, is governed by the replacement of Cl^- by H_2O in aqueous media. In fact, TD-DFT calculations reveal that in MeOH, where the Re(I) complex has the $[ClRe(CO)_3(BCS)]^{2-}$ structure, the relevant singlet−singlet electronic transitions leading to the population of the emitting ^{1}IL and ^{3}MLLCT excited states are H → L + 1 (at 358.2 nm), H − 1 → L (at 390.9 nm) and H − 1 → L + 1 (at 346.0 nm). The corresponding charge transfer percentages (% CT) for those electronic transitions are 47, 37 and 38% for H → L + 1, H − 1 → L and H − 1 → L + 1, respectively. Under the PCM, replacement of MeOH by H_2O with the same Re(I) complex structure has minimal effects on the calculated TD-DFT electronic transitions, i.e. H → L + 1 (at 357.5 nm), H − 1 → L (at 389.9 nm) and H − 1 → L + 1 (at 345.2 nm) are obtained with nearly the same f_{osc} as in the case of PCM/MeOH. On the other hand, TD-DFT calculations of the $[(H_2O)Re(CO)_3(BCS)]^-$/PCM/H_2O system show significant differences when compared to TD-DFT calculations with $[ClRe(CO)_3(BCS)]^{2-}$/PCM/MeOH. For $[(H_2O)Re(CO)_3(BCS)]^-$/PCM/H_2O, the relevant singlet−singlet electronic transitions leading to the population of the emitting ^{1}IL and ^{3}MLLCT excited states are H → L (at 385.7 nm) and H → L + 1 (at 337.2 nm), with 25 and 27% of CT, respectively. Moreover, the significant decrease of the % CT when passing from $[ClRe(CO)_3(BCS)]^{2-}$ to $[(H_2O)Re(CO)_3(BCS)]^-$ is in agreement with the increase of IL character of HOMO in $[(H_2O)Re(CO)_3(BCS)]^-$ (See Table 2) relative to $[ClRe(CO)_3(BCS)]^{2-}$. Therefore, the balance between ^{3}MLLCT and ^{1}IL is inclined toward the latter in aqueous solutions and the luminescence of the Re(I) complex is governed by ^{1}IL states. In the organic solvents, however, the outcome is the opposite and the photophysical properties of the Re(I) complex are dictated by ^{3}MLLCT excited states.

Singlet Oxygen Generation and LIOAS Experiments. Singlet oxygen generation by the Re(I) complex in both D_2O and acetonitrile solutions were analyzed by time-resolved phosphorescence measurements. The phosphorescence of

dx.doi.org/10.1021/jp506890r | J. Phys. Chem. A 2014, 118, 9661−9674

CH_3CN solutions showed clear evidence of singlet oxygen formation. Nevertheless, singlet oxygen generation in D_2O solutions could not be detected under our experimental conditions. Linear correlations were obtained from the plots of the dependence of the singlet oxygen phosphorescence intensity emission at zero time, S(0), as a function of the laser energy, for the complex and the reference. From these slopes and the usual procedure described elsewhere[73] the determined quantum yield of $O_2(^1\Delta_g)$ production was $\Phi_\Delta = 0.50 \pm 0.05$ and $\Phi_\Delta \leq 0.05$ in CH_3CN and D_2O, respectively.

The photophysical and photochemical pathways of eqs 9−12 have to be considered in order to find an expression for Φ_Δ as a function of the excited-state parameters of the sensitizer. $XRe(CO)_3L$ complexes may be used as sensitizers in the presence of oxygen, and $^1O_2$ ($^1\Delta_g$) may be produced by energy transfer from the ^3S (^{3}MLLCT) to molecular oxygen. The quenching mechanism of the excited triplet state of a sensitizer S by oxygen has been previously reported,[74] eq 13

$$^3S^* + {}^3O_2 \underset{k_{-d}}{\overset{k_d}{\rightleftarrows}} {}^{1,3,5}(^3S^* \ldots {}^3O_2) \xrightarrow{k_D} \begin{cases} \xrightarrow{k_\Delta} {}^1S + {}^1O_2 \\ \xrightarrow{k_{Td}} {}^1S + {}^3O_2 \end{cases} \quad (13)$$

In the first step of the quenching, the excited sensitizer $^3S^*$ and $^3O_2$ diffuse together to form the excited encounter complexes $^{1,3,5}(^3S^* \ldots {}^3O_2)$ with spin multiplicity m = 1, 3, and 5 and with a diffusion-controlled rate constant k_d. These complexes dissociate with rate constant k_{-d} or react to yield $^1O_2$ (either $^1\Delta_g$or $^1\Sigma_g^+$) or $^3O_2$. The quintet complex, $^5(^3S^* \ldots {}^3O_2)$, has no direct product channel.[71] k_Δ stands for the rate constant of the energy transfer process from ^3S to yield $^1O_2$ and k_{Td} represents the catalyzed triplet decay by molecular oxygen and $k_D = k_\Delta + k_{Td}$. The quantum yield of singlet oxygen production (Φ_Δ) is given by eqs 14−16:

$$\Phi_\Delta = \Phi_T P_{O_2}^T f_{O_2}^T \quad (14)$$

$$P_{O_2}^T = \frac{k_q[O_2]}{k_r + k_{nr} + k_q[O_2]} = \tau k_q[O_2] = 1 - \frac{\tau}{\tau_0} = 1 - \frac{I}{I_0} \quad (15)$$

$$f_{O_2}^T = \frac{k_\Delta}{k_D} \quad (16)$$

where Φ_T is the quantum yield of triplet formation; $P_{O_2}^T$ is the proportion of triplet states quenched by O_2; $f_{O_2}^T$ is the fraction of triplet states quenched by O_2 which yield $^1O_2$ ($^1\Delta_g$) (also named as the efficiency of singlet oxygen formation); k_q is the total quenching rate constant of triplet state by oxygen; τ_0 and τ are the triplet lifetimes in the absence and in the presence of oxygen, respectively. The mechanism was originally derived for singlet oxygen generation from the triplet states of organic sensitizers, and therefore ISC between the complexes $^{1,3,5}(^3S^* \ldots {}^3O_2)$ of different spin multiplicity was not taken into account.[75] By using the luminescence lifetimes in N_2 and in air, the value of $P_{O_2}^T$ calculated in CH_3CN solutions yields $P_{O_2}^T = 0.46$. Since it has been reported that Φ_T is unity due to the high degree of spin−orbit coupling in such heavy metal systems,[76] when compared to Φ_Δ, this $P_{O_2}^T$ value reflects essentially that $f_{O_2}^T$ is unity. Since k_d in acetonitrile is around 3×10^{10} M^{-1} s^{-1},[37,41] the value of k_q obtained for the complex is $\leq {}^1/_9 k_d$. Therefore, a predominance of the singlet channel in the mechanism of singlet oxygen generation was observed when this complex was used as photosensitizer.[13,39]

The overall rate constant k_D is calculated from experimental k_q by eq 17:

$$k_D = \frac{k_{-d} k_q}{k_d - k_q} \quad (17)$$

The dissociative rate constant, k_{-d}, is calculated according to k_{-d}/k_d = 1 M, where M is the unit mole per litter.[71] The calculated value of k_D is 2.6×10^9 M^{-1} s^{-1}. The multiplicity-normalized rate constants, $k_{\Delta E}^{nCT}/m$ (i.e., $k_{\Delta E}^{1\Sigma}/1$, $k_{\Delta E}^{1\Delta}/1$ and $k_{\Delta E}^{3\Sigma}/3$) depend for $^3S^*$ sensitizers with high oxidation potentials and minimum CT interactions between $^3S^*$ and O_2 on the excess energy (ΔE) for formation of $^1O_2$ ($^1\Sigma_g^+$), $^1O_2$ ($^1\Delta_g$) and $^3O_2$ ($^3\Sigma_g^-$) in a common way.[71] With the known value of the triplet sensitizer energy, the absolute contribution from the non charge-transfer path (nCT) to deactivation, eq 18, can be calculated with the aid of the polynomial expression of eq 19 via the corresponding excess energies ΔE (in kJ/mol):[71]

$$k_{\Delta E}^{nCT} = k_{\Delta E}^{1\Sigma} + k_{\Delta E}^{1\Delta} + k_{\Delta E}^{3\Sigma} \quad (18)$$

$$\log(k_{\Delta E}^{nCT}/m\ s^{-1}) = 9.05 + 9 \times 10^{-3}\Delta E - 1.15 \times 10^{-4}\Delta E^2 + 1.15 \times 10^{-7}\Delta E^3 + 9.1 \times 10^{-11}\Delta E^4 \quad (19)$$

where the excess energies are $\Delta E = E_T - 157$, $\Delta E = E_T - 94$ and $\Delta E = E_T = 207.7$ (λ_{em} = 576 nm in CH_3CN) for log ($k_{\Delta E}^{1\Sigma}$), log ($k_{\Delta E}^{1\Delta}$) and log ($k_{\Delta E}^{3\Sigma}$), respectively.[71] The relative importance between charge-transfer (CT) and non charge-transfer (nCT) deactivation mechanisms can be assessed by the quantity pCT which is defined, by eq 20, as the relative weight of charge transfer deactivation referred to the overall deactivation of the excited state by O_2.

$$p\mathrm{CT} = \frac{k_D - k_{\Delta E}^{nCT}}{k_D} \quad (20)$$

The calculated value of $k_{\Delta E}^{nCT}$ is 2.1×10^9 s^{-1}. Thus, the calculated values of $k_{\Delta E}^{nCT}$ are very close to the experimental k_D, with pCT ∼ 0.11, implying a dominance of the nCT mechanism in the overall deactivation of the excited state by O_2.

The fact that $^1O_2$ ($^1\Delta_g$) is not generated in aqueous solutions is related to two factors: (i) the low ^{3}MLLCT emission (note that in Table 4 Φ_{em}(Sp3) is always below 5×10^{-3}) and (ii) the low proportion of triplet states quenched by O_2 in that solvent (a value of only $P_{O_2}^T = 0.09$ can be calculated from luminescence lifetimes of Table 3). This is in agreement with our previous results in relation to the photosensitized generation of singlet oxygen from structurally related Re(I) complexes: $^1O_2$ ($^1\Delta_g$) generation was not observed when the luminescence quantum yields of the Re(I) complexes were as low as $\Phi_{em} \sim 10^{-3}$.[28]

We turn now to LIOAS experiments. The photoacoustic signal in both solvents showed the same behavior: no time shift or changes of shape, with respect to the calorimetric reference signal (See inset of Figure 9 for aqueous buffer solutions). Linear relationships in both solvents were obtained between the amplitude of the first optoacoustic signal (H) and the excitation fluence (F) for samples and references at various A, in a fluence range between 1 and 30 J/m^2. The ratio between the slopes of these lines for sample and reference yielded the values of α for

dx.doi.org/10.1021/jp506890r | J. Phys. Chem. A 2014, 118, 9661−9674

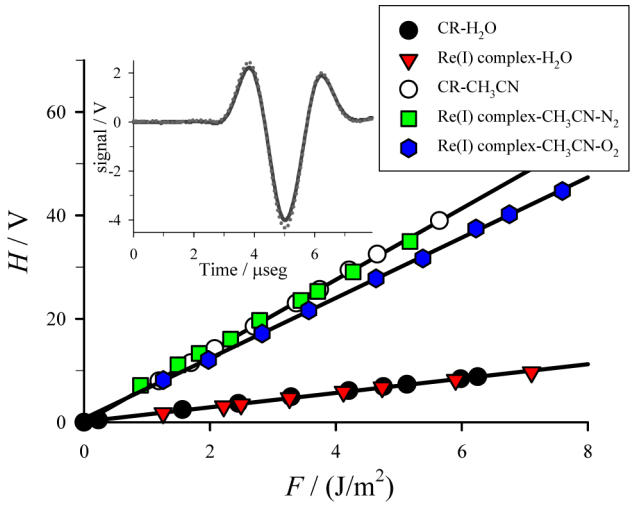

Figure 9. Amplitude of the photoacoustic signals as a function of laser fluence for (i) aqueous buffer solutions at pH = 7.0: New Coccine (CR, ●), Re(I) complex (red ▼) and (ii) CH_3CN solutions: 2-Hydroxybenzophenone (CR, ○), Re(I) complex (N_2, green ■; O_2, blue ⬢). Inset: Normalized photoacoustic signals of buffer solutions at pH = 7.0 for the CR (New Coccine, dotted line) and the Re(I) complex (solid line) with matched absorbances (0.105 ± 0.001).

the samples. For the complex in CH_3CN solution, see Figure 9, the slopes depended on the specific atmosphere and were different from the CR in the presence of oxygen, while for the aqueous solutions they were independent of the O_2 concentration. From these plots, considering that $\alpha_R = 1$ for CR, the α values were calculated for the complex in both solvents. For the case of buffer aqueous solutions, the slope obtained was the same that the CR measured at the same experimental conditions, as shown in Figure 9. A similar behavior was observed for deoxygenated CH_3CN solutions. Therefore, $\alpha = 1.00 \pm 0.04$ were obtained in aqueous solutions (either under N_2 or O_2 atmosphere) and in CH_3CN under N_2 atmosphere. Consequently, in these conditions, this complex released to the medium all the absorbed energy as prompt heat (integrated by the transducer) in processes faster than $\tau_R/5$. For the oxygen saturated CH_3CN solutions, the slopes observed in the plots of H vs F were lower than the CR ones, and the α value obtained was $\alpha = 0.86 \pm 0.05$. These values combined with fluorescence data and singlet oxygen quantum yield production fit the energy balance of eq 21:

$$E_a = \Phi_{em}E_{em} + \alpha E_a + \Phi_{st}E_{st} \quad (21)$$

where E_{em} is the 0−0 luminescence energy, E_a is the molar energy of the laser pulse (hc/λ_{exc}), E_{st} is the molar energy content of the species formed with a quantum yield Φ_{st} which stores energy for a time longer than the heat integration time and decays with a lifetime τ. When singlet oxygen acts as storing species, the corresponding values for this species are $\Phi_{em} \approx 0$, $\Phi_{st} = \Phi_\Delta$ and $\tau = \tau_\Delta$. Since in acetonitrile $\tau_\Delta \sim 40$ μs,[74] $^1O_2$ ($^1\Delta_g$) acts as an energy store within the time resolution of the LIOAS experiment.

CONCLUSIONS

Steady state and time-resolved luminescence and calorimetric studies, as well as TD-DFT calculations, reveal that the photophysical properties of the $[ClRe(CO)_3(BCS)]^{2-}$ complex are governed by the interplay between ^{3}MLLCT and ^{1}IL states. In organic solvents like CH_3CN or MeOH, ^{3}MLLCT states prevail and the usual expected behavior is observed: bathochromic shift of the emission maximum, a reduced luminescence quantum yield and the shortening of the excited-state lifetime upon increasing the polarity of the solvent system. In addition, $^1O_2$ is generated with high quantum yields by the quenching of the ^{3}MLLCT luminescence by $^3O_2$. In CH_3CN, the fraction of triplet states quenched by O_2 which yield $^1O_2$ is nearly unity. In aqueous solutions, however, due to the hydrolysis of the Re(I) complex, the replacement of Cl^- by H_2O in the metal coordination sphere alters the photophysical behavior dramatically. The contribution of ^{3}MLLCT luminescence to Φ_{em} drops and ^{1}IL states govern the photophysical behavior. A direct consequence is that $^1O_2$ is not detected in D_2O solutions. Moreover, the variation of the pH of the solution tunes the photophysical properties of the Re(I) complex by changing the relative amounts of $[ClRe(CO)_3(BCS)]^{2-}$, $[(OH)Re(CO)_3(BCS)]^{2-}$ and $[(H_2O)Re(CO)_3(BCS)]^-$ species. Decreasing the pH of the solution from 7.0 to 2.0 produces a remarkable increase in the luminescence quantum yield by nearly a 6-fold. TD-DFT calculations of the $[(H_2O)Re(CO)_3(BCS)]^-$/PCM/H_2O system show a significant decrease in the charge transfer percentages for the main electronic transitions when compared to $[ClRe(CO)_3(BCS)]^{2-}$/PCM/MeOH, in agreement with the increase of IL character of HOMO in $[(H_2O)Re(CO)_3(BCS)]^-$ relative to $[ClRe(CO)_3(BCS)]^{2-}$. Therefore, the balance between ^{3}MLLCT and ^{1}IL is inclined toward the latter in aqueous solutions and the luminescence of the Re(I) complex is governed by ^{1}IL states. In the organic solvents, however, the outcome is the opposite and the photophysical properties of the Re(I) complex are dictated by ^{3}MLLCT excited states.

AUTHOR INFORMATION

Corresponding Authors

*(E.W.) Telephone: +54 221 425-7430. E-mail: ewolcan@inifta.unlp.edu.ar.

*(P.M.D.G.) Telephone: +54 221 484-0280. E-mail: pedrodg@ciop.unlp.edu.ar.

Notes

The authors declare no competing financial interest.

ACKNOWLEDGMENTS

This work was supported in part by ANPCyT (PICT 1435), CONICET (PIP 0389), and Universidad Nacional de La Plata (UNLP X533 and X611) of Argentina. H.H.M.S. and F.R. thank CONICET for research scholarships. G.T.R. and E.W. are Research Members of CONICET (Argentina). P.M.D.G is a Research Member of CICBA (Argentina).

REFERENCES

(1) Vlček, A. Ultrafast Excited-State Processes in Re(I) Carbonyl-Diimine Complexes: From Excitation to Photochemistry. In *Photophysics of Organometallics*, Lees, A. J., Ed.; Springer: Berlin and Heidelberg, Germany, 2010; Vol. *29*, pp 73−114.

(2) Kumar, A.; Sun, S.-S.; Lees, A. Photophysics and Photochemistry of Organometallic Rhenium Diimine Complexes. In *Photophysics of Organometallics*, Lees, A. J., Ed.; Springer: Berlin and Heidelberg, Germany, 2010; Vol. *29*, pp 37−71.

(3) Fox, M. A.; Chanon, M. *Photoinduced Electron Transfer*; Elsevier: Amsterdam, 1988.

(4) Balzani, V.; Bolletta, F.; Gandolfi, M.; Maestri, M. Bimolecular Electron Transfer Reactions of the Excited States of Transition Metal Complexes. In *Organic Chemistry and Theory*; Springer: Berlin and Heidelberg, Germany, 1978; Vol. *75*, pp 1−64.
(5) Grätzel, M. *Energy Resources Through Photochemistry and Catalysis*; Academic Press: New York, 1983.
(6) Kalyanasundaram, K. Photophysics, Photochemistry and Solar Energy Conversion with Tris(Bipyridyl)Ruthenium(II) and Its Analogues. *Coord. Chem. Rev.* **1982**, *46*, 159−244.
(7) Kalyanasundaram, K.; Grätzel, M. *Photosensitization and Photocatalysis Using Inorganic and Organometallic Compounds*; Kluwer Academic Publishers: Dordrecht, The Netherlands, 1993.
(8) Sacksteder, L.; Lee, M.; Demas, J. N.; DeGraff, B. A. Long-Lived, Highly Luminescent Rhenium(I) Complexes as Molecular Probes: Intra- and Intermolecular Excited-State Interactions. *J. Am. Chem. Soc.* **1993**, *115*, 8230−8238.
(9) Yam, V. W.-W.; Wong, K. M.-C.; Lee, V. W.-M.; Lo, K. K.-W.; Cheung, K.-K. Synthesis, Photophysics, Ion-Binding Studies, and Structural Characterization of Organometallic Rhenium(I) Crown Complexes. *Organometallics* **1995**, *14*, 4034−4036.
(10) Yoon, D. I.; Berg-Brennan, C. A.; Lu, H.; Hupp, J. T. Synthesis and Preliminary Photophysical Studies of Intramolecular Electron Transfer in Crown-Linked Donor- (Chromophore-) Acceptor Complexes. *Inorg. Chem.* **1992**, *31*, 3192−3194.
(11) Calabrese, J. C.; Tam, W. Organometallics for Non-Linear Optics: Metal-Pyridine and Bipyridine Complexes. *Chem. Phys. Lett.* **1987**, *133*, 244−245.
(12) Ehler, T. T.; Malmberg, N.; Carron, K.; Sullivan, B. P.; Noe, L. J. Studies of Organometallic Self-Assembled Monolayers on Ag and Au Using Surface Plasmon Spectroscopy. *J. Phys. Chem. B* **1997**, *101*, 3174−3180.
(13) Louie, M.-W.; Fong, T. T.-H.; Lo, K. K.-W. Luminescent Rhenium(I) Polypyridine Fluorous Complexes as Novel Trifunctional Biological Probes. *Inorg. Chem.* **2011**, *50*, 9465−9471.
(14) Lo, K. Exploitation of Luminescent Organometallic Rhenium(I) and Iridium(III) Complexes in Biological Studies. In *Photophysics of Organometallics*; Lees, A. J., Ed. Springer: Berlin/Heidelberg, 2010; Vol. *29*, pp 73−114.
(15) Lo, K. K.-W.; Choi, A. W.-T.; Law, W. H.-T. Applications of Luminescent Inorganic and Organometallic Transition Metal Complexes as Biomolecular and Cellular Probes. *Dalton Trans.* **2012**, *41*, 6021−6047.
(16) Moya, S. A.; Guerrero, J.; Rodriguez-Nieto, F. J.; Wolcan, E.; Féliz, M. R.; Baggio, R. F.; Garland, M. T. Influence of the 4-Substituted Pyridine Ligand L′ on Both the Conformation and Spectroscopic Properties of the (2,2′-Biquinoline-κN^1,$\kappa N^{1'}$). *Helv. Chim. Acta* **2005**, *88*, 2842−2860.
(17) Bhuvaneswari, J.; Fathima, A. K.; Rajagopal, S. Rhenium(I)-Based Fluorescence Resonance Energy Transfer Probe for Conformational Changes of Bovine Serum Albumin. *J. Photochem. Photobiol., A* **2012**, *227*, 38−44.
(18) Cattaneo, M.; Fagalde, F.; Borsarelli, C. D.; Katz, N. E. Improvement of the Dynamic Range of pH Sensing by Using a Luminescent Tricarbonylpolypyridylrhenium(I) Complex with Three Different Protonation Sites. *Inorg. Chem.* **2009**, *48*, 3012−3017.
(19) Cattaneo, M.; Fagalde, F.; Katz, N. E. Proton-Induced Luminescence of Mono- and Dinuclear Rhenium(I) Tricarbonyl Complexes Containing 4-Pyridinealdazine. *Inorg. Chem.* **2006**, *45*, 6884−6891.
(20) Cattaneo, M.; Fagalde, F.; Katz, N. E.; Borsarelli, C. D.; Parella, T. pH-Induced Luminescence Changes of Chromophore-Quencher Tricarbonylpolypyridylrhenium(I) Complexes with 4-Pyridinealdazine. *Eur. J. Inorg. Chem.* **2007**, *2007*, 5309−5309.
(21) Higgins, B.; DeGraff, B. A.; Demas, J. N. Luminescent Transition Metal Complexes as Sensors: Structural Effects on pH Response. *Inorg. Chem.* **2005**, *44*, 6662−6669.
(22) Lin, R.-J.; Lin, K.-S.; Chang, I. J. Photophysical Properties of Tricarbonyl(Histidine)(Diimine)Rhenium(I) Complexes in Aqueous Solution. *Inorg. Chim. Acta* **1996**, *242*, 179−183.
(23) Bottorff, S. C.; Moore, A. L.; Wemple, A. R.; Bučar, D.-K.; MacGillivray, L. R.; Benny, P. D. pH-Controlled Coordination Mode Rearrangements of "Clickable" Huisgen-Based Multidentate Ligands with $[M^I(CO)_3]^+$ (M = Re, ^{99m}Tc). *Inorg. Chem.* **2013**, *52*, 2939−2950.
(24) Ragone, F.; Ruiz, G. T.; Piro, O. E.; Echeverría, G. A.; Cabrerizo, F. M.; Petroselli, G.; Erra-Balsells, R.; Hiraoka, K.; García Einschlag, F. S.; Wolcan, E. Water-Soluble (Pterin)Rhenium(I) Complex: Synthesis, Structural Characterization, and Two Reversible Protonation−Deprotonation Behavior in Aqueous Solutions. *Eur. J. Inorg. Chem.* **2012**, *2012*, 4801−4810.
(25) Martinez Saavedra, H. H.; Franca, C. A.; Petroselli, G.; Erra-Balsells, R.; Ruiz, G. T.; Wolcan, E. A New Zwitterionic, Water Soluble, Re(I) Complex: Synthesis, Spectroscopic and Computational Characterization. *J. Organomet. Chem.* **2013**, *745*−*746*, 470−478.
(26) Haas, K. L.; Franz, K. J. Application of Metal Coordination Chemistry to Explore and Manipulate Cell Biology. *Chem. Rev.* **2009**, *109*, 4921−4960.
(27) Ruiz, G. T.; Juliarena, M. P.; Wolcan, E.; Ferraudi, G. Kinetic and spectroscopic observations on the azidyl, $N_3^{\cdot}$, radical oxidation of fac-$(L_{spectator})Re^I(CO)_3(L_{acceptor})$ to fac-$(L_{spectator})Re^{II}(CO)_3(L_{acceptor})$, $L_{spectator}$ = 4,4′-bpy; $L_{acceptor}$ = dipyridyl[3,2-a:2′3′-c]phenazine or $L_{spectator} = Cl^-$; $L_{acceptor}$ = bathocuproindisulfonate: A revisitation to the self-exchange rate constants of the $N_3^{\cdot}/N_3^-$ and Re(II)/Re(I) couples and to the redox potential of the $N_3^{\cdot}$ radical. *Inorg. Chim. Acta* **2007**, *360*, 3681−3687.
(28) Ragone, F.; Martinez Saavedra, H. H.; David Gara, P. M.; Ruiz, G. T.; Wolcan, E. Photosensitized Generation of Singlet Oxygen from Re(I) Complexes: A Photophysical Study Using Lioas and Luminescence Techniques. *J. Phys. Chem. A* **2013**, *117*, 4428−4435.
(29) Braslavsky, S. E.; Heibel, G. E. Time-Resolved Photothermal and Photoacoustic Methods Applied to Photoinduced Processes in Solution. *Chem. Rev.* **1992**, *92*, 1381−1410.
(30) Van Haver, P.; Viaene, L.; Van der Auweraer, M.; De Schryver, F. C. References for Laser-Induced Opto-Acoustic Spectroscopy Using Uv Excitation. *J. Photochem. Photobiol., A* **1992**, *63*, 265−277.
(31) Abbruzzetti, S.; Viappiani, C.; Murgida, D. H.; Erra-Balsells, R.; Bilmes, G. M. Non-Toxic, Water-Soluble Photocalorimetric Reference Compounds for Uv and Visible Excitation. *Chem. Phys. Lett.* **1999**, *304*, 167−172.
(32) Schmidt, R.; Tanielian, C.; Dunsbach, R.; Wolff, C. Phenalenone, a Universal Reference Compound for the Determination of Quantum Yields of Singlet Oxygen O_2 ($^1\Delta g$) Sensitization. *J. Photochem. Photobiol., A* **1994**, *79*, 11−17.
(33) San Roman, E.; Gonzalez, M. C. Analysis of Spectrally Resolved Kinetic Data and Time-Resolved Spectra by Bilinear Regression. *J. Phys. Chem.* **1989**, *93*, 3532−3536.
(34) Gao, Y.; Sun, S.; Han, K. Electronic Structures and Spectroscopic Properties of Rhenium (I) Tricarbonyl Photosensitizer: $[Re(4,4'\text{-}(COOEt)2\text{−}2,2'\text{-}Bpy)(CO)_3py]PF_6$. *Spectrochim. Acta, Part A* **2009**, *71*, 2016−2022.
(35) Vlcek, A., Jr; Zális, S. Modeling of Charge-Transfer Transitions and Excited States in d6 Transition Metal Complexes by DFT Techniques. *Coord. Chem. Rev.* **2007**, *251*, 258−287.
(36) Dietrich, J.; Thorenz, U.; Förster, C.; Heinze, K. Effects of Sequence, Connectivity, and Counter Ions in New Amide-Linked $Ru(Tpy)_2$−Re(Bpy) Chromophores on Redox Chemistry and Photophysics. *Inorg. Chem.* **2013**, *52*, 1248−1264.
(37) Chartrand, D.; Castro Ruiz, C. A.; Hanan, G. S. Diimine Triscarbonyl Re(I) of Isomeric Pyridyl-Fulvene Ligands: An Electrochemical, Spectroscopic, and Computational Investigation. *Inorg. Chem.* **2012**, *51*, 12738−12747.
(38) Zhao, C.; Kambara, C. S.; Yang, Y.; Kaledin, A. L.; Musaev, D. G.; Lian, T.; Hill, C. L. Synthesis, Structures, and Photochemistry of Tricarbonyl Metal Polyoxoanion Complexes, $[X_2W_{20}O_{70}\{M(CO)_3\}_2]^{12-}$ (X = Sb, Bi and M = Re, Mn). *Inorg. Chem.* **2013**, *52*, 671−678.
(39) Anderson, C. B.; Elliott, A. B. S.; McAdam, C. J.; Gordon, K. C.; Crowley, J. D. Fac-$Re(CO)_3Cl$ Complexes of [2-(4-R-1h-1,2,3-Triazol-

1-Yl)Methyl]Pyridine Inverse "Click" Ligands: A Systematic Synthetic, Spectroscopic, and Computational Study. *Organometallics* **2013**, *32*, 788−797.
(40) Yang, L.; Ren, A.-M.; Feng, J.-K.; Liu, X.-D.; Ma, Y.-G.; Zhang, H.-X. Theoretical Studies of Ground and Excited Electronic States in a Series of Rhenium(I) Bipyridine Complexes Containing Diarylethynyl-Based Structure. *Inorg. Chem.* **2004**, *43*, 5961−5972.
(41) Yang, L.; Ren, A.-M.; Feng, J.-K.; Liu, X.-J.; Ma, Y.-G.; Zhang, M.; Liu, X.-D.; Shen, J.-C.; Zhang, H.-X. Theoretical Studies of Ground and Excited Electronic States in a Series of Halide Rhenium(I) Bipyridine Complexes. *J. Phys. Chem. A* **2004**, *108*, 6797−6808.
(42) Záliš, S.; Milne, C. J.; El Nahhas, A.; Blanco-Rodríguez, A. M.; van der Veen, R. M.; Vlček, A. Re and Br X-Ray Absorption near-Edge Structure Study of the Ground and Excited States of [ReBr-$(CO)_3$(Bpy)] Interpreted by DFT and TD-DFT Calculations. *Inorg. Chem.* **2013**, *52*, 5775−5785.
(43) Bossert, J.; Daniel, C. Trans−Cis Photoisomerization of the Styrylpyridine Ligand in $[Re(CO)_3$(2,2′-Bipyridine)(T-4-Styrylpyridine)$]^+$: Role of the Metal-to-Ligand Charge-Transfer Excited States. *Chem.—Eur. J.* **2006**, *12*, 4835−4843.
(44) Hohenberg, P.; Kohn, W. Inhomogeneous Electron Gas. *Phys. Rev.* **1964**, *136*, B864−B871.
(45) Kohn, W.; Sham, L. J. Self-Consistent Equations Including Exchange and Correlation Effects. *Phys. Rev.* **1965**, *140*, A1133−A1138.
(46) Parr, R. G.; Yang, W. *Density Functional Theory of Atoms and Molecules*. Oxford University Press: Oxford, U.K., 1989.
(47) Frisch, M. J.; Trucks, G. W.; Schlegel, H. B.; Scuseria, G. E.; Robb, M. A.; Cheeseman, J. R.; Scalmani, G.; Barone, V.; Mennucci, B.; Petersson, G. A.; et al.. *Gaussian 09, Revision A1*; Gaussian, Inc.: Wallingford CT, 2009.
(48) Becke, A. D. Density-Functional Thermochemistry. III. The Role of Exact Exchange. *J. Chem. Phys.* **1993**, *98*, 5648−5652.
(49) Lee, C.; Yang, W.; Parr, R. G. Development of the Colle-Salvetti Correlation-Energy Formula into a Functional of the Electron Density. *Phys. Rev. B* **1988**, *37*, 785−789.
(50) Dunning-Jr, T. H.; Hay, P. J. *Methods of Electronic Structure Theory*. Schaefer, H. F., III, Ed.; Plenum Press: London, 1977; Vol. 2.
(51) Hay, P. J.; Wadt, W. R. Ab Initio Effective Core Potentials for Molecular Calculations. Potentials for the Transition Metal Atoms Sc to Hg. *J. Chem. Phys.* **1985**, *82*, 270−283.
(52) Hay, P. J.; Wadt, W. R. Ab Initio Effective Core Potentials for Molecular Calculations. Potentials for K to Au Including the Outermost Core Orbitals. *J. Chem. Phys.* **1985**, *82*, 299−310.
(53) Wadt, W. R.; Hay, P. J. Ab Initio Effective Core Potentials for Molecular Calculations. Potentials for Main Group Elements Na to Bi. *J. Chem. Phys.* **1985**, *82*, 284−298.
(54) Bauernschmitt, R.; Ahlrichs, R. Treatment of Electronic Excitations within the Adiabatic Approximation of Time Dependent Density Functional Theory. *Chem. Phys. Lett.* **1996**, *256*, 454−464.
(55) Casida, M. E.; Jamorski, C.; Casida, K. C.; Salahub, D. R. Molecular Excitation Energies to High-Lying Bound States from Time-Dependent Density-Functional Response Theory: Characterization and Correction of the Time-Dependent Local Density Approximation Ionization Threshold. *J. Chem. Phys.* **1998**, *108*, 4439−4449.
(56) Stratmann, R. E.; Scuseria, G. E.; Frisch, M. J. An Efficient Implementation of Time-Dependent Density-Functional Theory for the Calculation of Excitation Energies of Large Molecules. *J. Chem. Phys.* **1998**, *109*, 8218−8224.
(57) Feller, D. The Role of Databases in Support of Computational Chemistry Calculations. *J. Comput. Chem.* **1996**, *17*, 1571−1586.
(58) Schuchardt, K. L.; Didier, B. T.; Elsethagen, T.; Sun, L.; Gurumoorthi, V.; Chase, J.; Li, J.; Windus, T. L. Basis Set Exchange: A Community Database for Computational Sciences. *J. Chem. Inf. Model.* **2007**, *47*, 1045−1052.
(59) Barone, V.; Cossi, M. Quantum Calculation of Molecular Energies and Energy Gradients in Solution by a Conductor Solvent Model. *J. Phys. Chem. A* **1998**, *102*, 1995−2001.
(60) Cossi, M.; Barone, V. Time-Dependent Density Functional Theory for Molecules in Liquid Solutions. *J. Chem. Phys.* **2001**, *115*, 4708−4717.
(61) Mennucci, B.; Tomasi, J. Continuum Solvation Models: A New Approach to the Problem of Solute's Charge Distribution and Cavity Boundaries. *J. Chem. Phys.* **1997**, *106*, 5151−5158.
(62) Gorelsky, S. I.; Lever, A. B. P. Electronic Structure and Spectra of Ruthenium Diimine Complexes by Density Functional Theory and Indo/S. Comparison of the Two Methods. *J. Organomet. Chem.* **2001**, *635*, 187−196.
(63) Gorelsky, S. I. *AOMix program, revision 6.81*, http://www.sg-chem.net/.
(64) Wolcan, E. On the Origins of the Absorption Spectroscopy of Pterin and $Re(CO)_3$(Pterin)(H_2O) Aqueous Solutions. A Combined Theoretical and Experimental Study. *Spectrochim. Acta, Part A* **2014**, *129*, 173−183.
(65) Fernández-Moreira, V.; Thorp-Greenwood, F. L.; Amoroso, A. J.; Cable, J.; Court, J. B.; Gray, V.; Hayes, A. J.; Jenkins, R. L.; Kariuki, B. M.; Lloyd, D.; et al. Uptake and Localisation of Rhenium Fac-Tricarbonyl Polypyridyls in Fluorescent Cell Imaging Experiments. *Org. Biomol. Chem.* **2010**, *8*, 3888−3901.
(66) Amoroso, A. J.; Coogan, M. P.; Dunne, J. E.; Fernández-Moreira, V.; Hess, J. B.; Hayes, A. J.; Lloyd, D.; Millet, C.; Pope, S. J. A.; Williams, C. Rhenium Fac Tricarbonyl Bisimine Complexes: Biologically Useful Fluorochromes for Cell Imaging Applications. *Chem. Commun.* **2007**, 3066−3068.
(67) Gorelsky, S. I.; Lever, A. B. P. The Electronic Structure and Spectra of $[Ru(NH_3)_4(L_l)]^{2+}$ (L_l = Bpy, Bpz, Bqdi) Studied by Density Functional Theory and Indo/S. Charge Transfer Character of Electronic Transitions and Their Solvatochromism. *Can. J. Anal. Sci. Spectrosc.* **2003**, *48*, 93−105.
(68) O'Boyle, N. *GaussSum 2.2.5 program documentation* (http://gausssum.sourceforge.net/GaussSum_UVVis_Convolution.pdf).
(69) Listorti, A.; Degli Esposti, A.; Kishore, R. S. K.; Kalsani, V.; Schmittel, M.; Armaroli, N. 1,10-Phenanthrolines with Tunable Luminescence Upon Protonation: A Spectroscopic and Computational Study. *J. Phys. Chem. A* **2007**, *111*, 7707−7718.
(70) Xiao, Z.; Brose, J.; Schimo, S.; Ackland, S. M.; La Fontaine, S.; Wedd, A. G. Unification of the Copper(I) Binding Affinities of the Metallo-Chaperones Atx1, Atox1, and Related Proteins: Detection Probes and Affinity Standards. *J. Biol. Chem.* **2011**, *286*, 11047−11055.
(71) Schmidt, R. The Effect of Solvent Polarity on the Balance between Charge Transfer and Non-Charge Transfer Pathways in the Sensitization of Singlet Oxygen by $\pi\pi^*$ Triplet States. *J. Phys. Chem. A* **2006**, *110*, 5990−5997.
(72) Battino, R.; Rettich, T. R.; Tominaga, T. The Solubility of Oxygen and Ozone in Liquids. *J. Phys. Chem. Ref. Data* **1983**, *12*, 163−178.
(73) Martí, C.; Jürgens, O.; Cuenca, O.; Casals, M.; Nonell, S. Aromatic Ketones as Standards for Singlet Molecular Oxygen $O_2(^1\Delta g)$ Photosensitization. Time-Resolved Photoacoustic and near-IR Emission Studies. *J. Photochem. Photobiol., A* **1996**, *97*, 11−18.
(74) Wilkinson, F.; Brummer, J. G. Rate Constants for the Decay and Reactions of the Lowest Electronically Excited Singlet State of Molecular Oxygen in Solution. *J. Phys. Chem. Ref. Data* **1981**, *10*, 809−999.
(75) Gijzeman, O. L. J.; Kaufman, F.; Porter, G. Oxygen Quenching of Aromatic Triplet States in Solution. Part 1. *J. Chem. Soc., Faraday Trans. 2: Mol. Chem. Phys.* **1973**, *69*, 708−720.
(76) Abdel-Shafi, A. A.; Bourdelande, J. L.; Ali, S. S. Photosensitized Generation of Singlet Oxygen from Rhenium(I) and Iridium(III) Complexes. *Dalton Trans.* **2007**, 2510−2516.